

Copyright
by
Krishnakumar Varadarajan
2003

**A STUDY OF THE EFFECTS OF A HOT STREAK ON FILM
COOLING EFFECTIVENESS IN A TURBINE VANE**

by

Krishnakumar Varadarajan, B.E.

Thesis

Presented to the Faculty of the Graduate School of

The University of Texas at Austin

in Partial Fulfillment

of the Requirements

for the Degree of

MASTER OF SCIENCE IN ENGINEERING

The University of Texas at Austin

MAY 2003

**A STUDY OF THE EFFECTS OF A HOT STREAK ON FILM
COOLING EFFECTIVENESS IN A TURBINE VANE**

**Approved by
Supervising Committee:**

David G. Bogard

Michael E. Crawford

To my Mom

ACKNOWLEDGEMENTS

I would like to thank Dr. David Bogard for his support and for all the time he spent to patiently teach me the various technical aspects. I would also like to appreciate the understanding he showed during my difficult times. I would like to thank Dr. Michael Crawford for reviewing my thesis. My thanks to Daniel Snook and Jay Hyatt for their help in getting me to understand the workings of all the equipment and the data reduction process. I thank Sean Jenkins for all the effort he put in and for all his help in my research. Thanks to Jason Albert for being the only person to really clean up the lab. Thanks to Elon Terrel and Jay Rutledge for helping me run various experiments. Thanks to David Robertson for helping us finally get the new equipment and getting it to work. I would also like to thank to Don Artieschoufsky, Danny Jares, Curtis Johnson, and John Pedracine for all their help in building all kinds of fixtures. I also would like to thank my dad and my friends for all their love and support.

May 2003

ABSTRACT

A STUDY OF THE EFFECTS OF A HOT STREAK ON FILM COOLING EFFECTIVENESS IN A TURBINE VANE

Krishnakumar Varadarajan, M.S.E.

The University of Texas at Austin, 2003

Supervisor: David G. Bogard

An experimental study was conducted in a simulated linear cascade to determine the effects of a hot streak on coolant effectiveness. The experiments also looked at the effects of mainstream turbulence and the effects of the vane on a hot streak. A hot streak generator section was installed in the tunnel to produce a hot streak temperature ratio, which was defined as the ratio of the maximum hot streak temperature to the mainstream temperature of 1.1 at $0.21C$ upstream of the vane leading edge. The temperature profiles measured in the wake at $0.32C$ downstream of the trailing edge demonstrated that the mainstream turbulence caused a considerable decay in the hot streak. The differences in the peak normalized temperature ratios between high mainstream turbulence ($Tu = 20\%$) and moderate mainstream turbulence ($Tu = 3.5\%$) was

only 20%. The adiabatic effectiveness tests were conducted in the showerhead region and in the suction side region. Temperature field measurements were made in the region close to the vane surface. From the adiabatic effectiveness experiments and the thermal field measurements, it was concluded that the mainstream temperature could be adjusted to scale the effectiveness levels properly. The adjusted mainstream temperature was equal to the hot streak temperature in the showerhead region, where the hot streak temperature was constant near the vane surface. For the suction side region, the hot streak temperature had a gradient near the wall. The surface temperatures of the vane with a hot streak and no film cooling provided the right scaling temperatures.

Table of Contents

List of Tables	xi
List of Figures	xii
NOMENCLATURE	xv
CHAPTER ONE	
INTRODUCTION	1
1.1 TURBINE COOLING	2
1.1.1 Coolant Jet Parameters	4
1.2 HOT STREAKS	6
1.2.1 Experimental Studies	7
1.2.2 Numerical Studies	10
1.3 OBJECTIVE OF CURRENT STUDY	14
CHAPTER TWO	
TEST FACILITY AND EXPERIMENTAL PROCEDURES	15
2.1 TEST FACILITY	15
2.1.1 Mainstream Flow Loop	15
2.1.2 Secondary Flow Loop	17
2.1.3 Test Section	18

2.1.4 Heater Section	19
2.1.5 Turbulence Generator	20
2.1.6 Test Airfoil	21
2.1.7 Surface Temperature Measurements	22
2.1.8 Thermocouple Rakes	23
2.2 EXPERIMENTAL PROCEDURE	24
2.2.1 Velocity Measurements	24
2.2.2 Turbulence Measurements	24
2.2.2 Effectiveness Tests	25
2.2.4 Hot Streak Measurements	29
2.3 DATA REDUCTION PROCESS	30
2.4 UNCERTAINTY ANALYSIS	32
2.4.1 Effectiveness Tests	32
2.4.2 Hot Streak Measurements	34

CHAPTER THREE

FLOW FIELD CONDITIONS AND HOT STREAK MEASUREMENTS	42
3.1 FLOW FIELD MEASUREMENTS	42
3.1.1 Velocity Measurements	42
3.1.2 Turbulence Measurements	44

3.2 HOT STREAK MEASUREMENTS	45
3.3 EFFECT OF THE VANE ON THE HOT STREAK	48
CHAPTER FOUR	
EXPERIMENTAL RESULTS	62
4.1 TEST CONDITIONS	62
4.2 SHOWERHEAD REGION	64
4.2.1 Moderate Mainstream Turbulence	65
4.2.2 High Mainstream Turbulence	67
4.3 SUCTION SIDE REGION	68
4.3.1 Moderate Mainstream Turbulence	68
4.3.2 High Mainstream Turbulence	74
CHAPTER FIVE	
CONCLUSIONS	88
5.1 SUMMARY OF RESULTS	88
5.2 RECOMMENDED FUTURE WORK	90
REFERENCES	91
VITA	95

List of Tables

4.1	Surface Temperature comparison at $x'/d = 7$	71
4.2	Surface Temperature comparison at $x'/d = 14$	71

List of Figures

2.1	Schematic of wind tunnel	36
2.2	Schematic of test section and the hot streak generator	37
2.3	Positions and sizes of the support rods and the resistance rods in the hot streak generator section	38
2.4	Test Vane with showerhead and pressure side film cooling holes	39
2.5	Schematic of Film cooling hole configurations	40
2.6	Sample Calibration Curve	41
3.1	Horizontal profile of the streamwise velocity measured at $0.14C$ upstream of the leading edge.	50
3.2	Vertical profile of the normalized velocity distribution measured at $0.21C$ upstream of the leading edge under moderate turbulence levels.	51
3.3	Vertical profile of the normalized velocity distribution measured at $0.21C$ upstream of the leading edge under high turbulence levels.	52
3.4	Vertical profile of the normalized velocity measurements made at a location $0.21C$ upstream of the leading edge across the heater under moderate turbulence with and without the hot streak.	53
3.5	Turbulence measurements made at a location $0.21C$ upstream of the leading edge under moderate turbulence conditions.	54
3.6	Turbulence measurements made at a location $0.21C$ upstream of the leading edge under high turbulence conditions.	55
3.7	Normalized temperature profiles measured at the reference and wake location under moderate turbulence.	56

3.8	Normalized temperature profiles measured at the reference and wake location under moderate turbulence.	57
3.9	Normalized temperature ratio plot in the wake at a location $0.32C$ from the trailing edge for the hot streak aimed through the passage for moderate and high turbulence	58
3.10	Normalized Temperature ratio plot measured in the wake at a location $0.32C$ from the leading edge under high turbulence for impacting and non impacting hot streak	59
3.11	Temperature profiles measured along the suction side with the hot streak impacting the vane.	60
3.12	Temperature profiles measured along the pressure side with the hot streak impacting the vane	61
4.1	Temperature ratio measured in the showerhead region under moderate turbulence showing the spanwise variations.	75
4.2	Temperature ratio measured in the showerhead region under moderate turbulence showing the streamwise variations.	75
4.3	Adiabatic effectiveness in the showerhead region at a $DR = 1.2$, $M = 2.0$ under moderate turbulence conditions with and without the hot streak	76
4.4	Adiabatic effectiveness in the showerhead region at a $DR = 1.2$, and $M = 1.0$ and $M = 1.6$ under moderate turbulence conditions with and without the hot streak	77
4.5	Contour levels of local effectiveness values in the showerhead under moderate turbulence condition without a hot streak	78
4.6	Contour levels of local effectiveness values in the showerhead under moderate turbulence condition with a hot streak	78
4.7	Temperature ratio measured in the showerhead region at $x/d = 0$ under high turbulence conditions showing the spanwise variations.	79
4.8	Temperature ratio measured in the showerhead region at $z = 0.47S$ under high turbulence conditions showing streamwise variations.	79
4.9	Temperature ratio measured on the suction side at $x'/d = 0$ with just the hot streak under moderate turbulence.	80

4.10	Temperature ratio measured on the suction side at $z = 0.51S$ with just the hot streak under moderate turbulence.	80
4.11	Temperature ratio measured on the suction side at $z = 0.51S$ and at $x'/d = 0$, with coolant at a density ratio of 1.2, without the presence of a hot streak.	81
4.12	Temperature ratio measured on the suction side at $z = 0.51S$ and at $x'/d = 0$, with coolant at a density ratio of 1.2 in the presence of a hot streak.	82
4.13	Comparison of vane surface temperature under the influence of a hot streak as measured by a thermocouple rake and as calculated using a curve fit of temperatures	83
4.14	Adiabatic Effectiveness in the suction side for 1 row of holes blowing at a density ratio of 1.2 and blowing ratio of 0.5 under moderate turbulence	84
4.15	Adiabatic Effectiveness in the suction side for 1 row of holes blowing at a density ratio of 1.2 under moderate turbulence for blowing ratios of 0.6 and 1.2	85
4.16	Contour levels of local effectiveness values in the suction side under moderate turbulence condition without the presence of a hot streak	86
4.17	Contour levels of local effectiveness values in the suction side under moderate turbulence condition with a hot streak using an “adjusted” temperature	86
4.18	Temperature ratio measured on the suction side at $0.51S$ with just the hot streak under high turbulence.	87

NOMENCLATURE

Symbols

C	vane chord length, 0.594 m
DR	density ratio, $\frac{\rho_c}{\rho_\infty}$
d	film cooling hole diameter, 4.11 mm
I	Momentum flux ratio, $\frac{\rho_c U_c^2}{\rho_\infty U_\infty^2}$
m	order of curve fit
M	blowing ratio, $\frac{\rho_c U_c}{\rho_\infty U_\infty}$
N	number of measurements
p	hole-to-hole pitch
P	pitch between vanes, 0.46 m
S	Airfoil Span , 0.54 m
Re	Reynolds number, $\frac{\rho U c}{\mu}$
T	temperature
Tu	turbulence intensity, $\frac{u_{rms}}{U}$
U	flow velocity
VR	velocity ratio, $\frac{U_c}{U_\infty}$
x	streamwise coordinate along the airfoil surface
y	distance across the tunnel along a line tangent to the airfoil surface at the location of the airfoil geometric leading edge

z spanwise coordinate

Greek Symbols

Λ_f integral length scale

η adiabatic effectiveness, $\frac{(T_\infty - T_{aw})}{(T_\infty - T_c)}$

η_0 conduction error

μ dynamic viscosity

Θ_R non-dimensional temperature, $\frac{T_{hs} - T_\infty}{T_{0,hs} - T_\infty}$

ρ density

σ standard deviation

ν kinematic viscosity

Subscripts

0 approach condition

1 at inlet to vane cascade

aw adiabatic wall

c coolant conditions

hs hot streak value

inlet inlet conditions

rms root-mean-square

SL streamline

∞ freestream conditions

Superscript

* Showerhead conditions

CHAPTER ONE

INTRODUCTION

Gas Turbine engines are commonly used for power generation. These engines are based on the Brayton cycle. The efficiency of this cycle, for a given pressure ratio and environmental conditions can be increased by increasing the maximum inlet temperature to the turbine. Modern gas turbine engines are thus designed with high turbine inlet temperatures to improve the efficiency of the cycle and help lower the fuel consumption. But the extent of the increase in the gas temperature is limited by the material limitations of the airfoil and has a direct impact on the durability of the vanes and blades. The present exit temperatures are already 300°C higher than the allowable metal melting temperature as reported by Han et al. (2000). The replacement and repair of blades and vanes are highly expensive and hence different techniques are required to help improve the life of the blades.

Thus there is a need to increase the exit temperatures of the combustor without destroying the vane or the blade. This has been achieved by the implementation of efficient cooling arrangements and high temperature alloys provided with a thermal barrier coating (TBC). But both these methods have their

own drawbacks. The use of TBC is limited by their degradation due to corrosion and oxidation. The use cooling techniques require the removal of air from the compressor which lowers the overall efficiency and aerodynamic losses caused by dumping the coolant into the mainstream. Thus there is a lot of research performed in this subject to better understand and implement these techniques in an effective manner.

1.1 TURBINE COOLING

Modern turbines use the concept of actively cooling the vanes by bleeding some cooler air from the later stages of the compressor. The cooling process has to be optimized as the extraction of air from the compressor results in a decrease in the thermal efficiency. Gas turbine vanes are cooled internally as well as externally. Internal cooling uses coolant air passed through several serpentine passages inside the vane to transfer the heat away from the surface of the vane. This cooling technique is more common in the mid chord region as described by Han et al. (2000). Usually the passages are ribbed to increase turbulence that helps improve the heat transfer.

Jet impingement cooling is another method which has a lot of potential to increase the heat transfer rates. This cooling is most commonly used in the leading edge of the rotor blades where the coolant requirements are the highest.

Based on structural constraints, this cooling is used more in the mid chord region in the case of stator vanes as described in Han et al. (2000). Most commonly, an array of jets is used in this method to improve the cooling performance. Pin fin cooling uses pin shaped fins that are oriented perpendicular to the flow direction to maximize forced convection fin cooling. Pin fin cooling is usually used in the trailing edge where structural constraints prevent the use of the other cooling configurations.

External film cooling introduces a film of secondary air or coolant on the surface of the vane to protect the surface from the high temperatures. Film cooling protects the airfoil directly and also removes heat from the surface through the cooling hole by internal convection. To provide a proper indicator of the cooling, both the airfoil surface temperatures and the heat transfer coefficients are required. The adiabatic effectiveness, η , is used to provide information on how well the coolant is able to protect the vane surface from the mainstream temperatures. It is a non-dimensional quantity defined as :

$$\eta = \frac{T_{aw} - T_{\infty}}{T_c - T_{\infty}} \quad (1.1)$$

Where T_{aw} represents the adiabatic wall temperature, T_{∞} represents the mainstream temperature and T_c represents the coolant temperature. Thus an

adiabatic effectiveness of $\eta = 0$ means that the vane surface temperature is the same as the mainstream temperature and the coolant was totally ineffective.

There are a number of factors that affect the performance of film cooling like injection angles, hole geometry, surface roughness and mass flow rate. The characteristics of the mainstream like Reynolds number, pressure gradients, turbulence intensities and so on also affect the overall performance. Certain other coolant jet parameters like density ratio, blowing ratio and momentum flux ratio are also important in evaluating the performance. A large number of experiments and numerical studies have been conducted to evaluate the effects of these parameters on film cooling effectiveness on flat plate geometries and vane models. Most of these studies were done without the presence of a hot streak. The various studies of hot streak, with most studies concentrating on the rotor, have also not looked at the effect of the hot streak on the coolant effectiveness in the vane. All the research in this thesis is concentrated on this subject.

1.1.1 Coolant Jet Parameters

The coolant jet is characterized by the density ratio between the coolant and the mainstream. The density ratio is defined as

$$DR = \frac{\rho_c}{\rho_\infty} \quad (1.2)$$

The density ratios that are common in jet engines are close to 2.0 as presented by Han et al. (2002). To achieve this density ratio in the laboratory, either a temperature difference is established between the coolant jet and the mainstream or two gases of different densities are used. In our laboratory, the first approach is followed. The mainstream is maintained at 300K, and the coolant is cooled cryogenically until the required ratio is obtained.

The performance of the coolant stream can then be characterized using a blowing ratio, momentum flux ratio or a velocity ratio. The momentum flux ratio is a measure of the momentum of the coolant jet relative to the momentum of the mainstream, and is defined as

$$I = \frac{\rho_c U_c^2}{\rho_\infty U_\infty^2} \quad (1.3)$$

where U_c is the average velocity of the jet at the hole exit.

The velocity ratio is a direct measure of the ratio of the coolant jet velocity between the coolant jet and the mainstream. It is defined as

$$VR = \frac{U_c}{U_\infty} \quad (1.4)$$

The blowing ratio is a mass flux ratio and is a measure of the mass flux of coolant injected with respect to the mass flux of the mainstream. It is defined as

$$M = \frac{\rho_c U_c}{\rho_\infty U_\infty} \quad (1.5)$$

All the above three parameters have been used to characterize the coolant jet in different regimes in the literature. For a fixed density ratio, all the parameters are interchangeable. In this thesis, the blowing ratio is used to characterize the coolant jet.

1.2 HOT STREAKS

In gas turbine engines, the flow exiting the combustor has been shown to have large circumferential and radial gradients of temperature as indicated by Butler et al. (1989). These temperature gradients results in hot streaks as they pass through the turbine stage. It is important to understand the heat loads on the components in the hot gas path to improve their efficiency and their durability. The temperature profiles and the associated turbulence levels at the exit of the combustor are important in determining the heat load distributions on the first stage vanes.

The strength of the hot streak is usually described in terms of a temperature ratio, which is a ratio of the maximum temperature of the hot streak to the mainstream temperature. Previous studies of hot streak have used temperature ratios varying from 1.1 to 2.0. Dorney (1997) had noted in his studies that temperature ratios varying from 1.1 to 1.6 are typical in an engine. The various experiments and numerical studies on this subject are reviewed.

1.2.1 Experimental Studies

There have been several experiments and numerical studies on hot streaks as highlighted by Dorney et al. (1999). Among some of the experimental studies, Schwab et al. (1983) and Stabe et al. (1984) performed studies at the NASA Lewis Research center. They conducted these tests with the use of a parabolic inlet temperature profile developed by the use of a Combustor Exit Radial Temperature Simulator (CERTS). The parabolic temperature profile was a reasonably realistic simulation of an actual hot streak. They conducted the experiments with a hot streak temperature ratio of 1.2 measured at a location less than one chord length upstream of the vane. As the measurements in these experiments were taken only on the rotor, there was no information available in the region just downstream of the stator. There are no specific turbulence levels mentioned although the description of the facility indicates low turbulence levels.

Butler et al. (1989) performed another experiment using the Large Scale Rotating Rig (LSRR) used at the United Technologies Research Center. This experiment introduced a hot streak which had both radial and circumferential gradients and had a realistic temperature profile. The hot streak had a temperature ratio of 2.0 and was introduced at the middle of the stator passage at a radial location that was 40% above the hub. The location of the temperature ratio

measurement was not stated. The diameter of the hot streak was about half the pitch distance between the vanes. The turbulence levels in this facility were around 1%. The hot streak was seeded with CO₂, and the concentration of CO₂ was used to relate to the temperature distributions and to monitor the movement and location of the hot streak. The measurements that were made on the rotor showed that the hot streak tended to migrate over to the pressure side and this was explained by the presence of secondary flows. These were generated by the development of streamwise vorticity caused by the inflow temperature non-uniformities. This experiment was the common benchmark for most of the numerical studies to follow.

Shang and Epstien (1996) later conducted heat transfer studies on the rotor at the same LSRR test facility. They introduced a hot streak with a diameter equal to pitch between the stator vanes with a temperature ratio of 1.1 but the measurement location of this temperature ratio is not mentioned. The heat transfer results obtained by these experiments again indicated the presence of secondary flows that were induced by temperature gradients as well as tip and clearance flows. Although, the heat transfer study was performed in a detailed manner, this was again on the rotor surface.

Roback and Dring (1993) performed a series of experiments at the LSRR where they measured the effects of the hot streak and stator trailing edge cooling

in the rotor passage. They used a hot streak with a diameter equal to one-third the pitch distance between the vanes that they introduce at the mid pitch between two stators and at different span heights. The hot streak also had a parabolic shaped temperature profile. These profiles were measured at the exit location of the streak injector. Measurements of the hot streak temperatures were also made at the rotor leading edge with the hot streak positioned to impact on the vane and the measured temperatures in the wake were similar to the values obtained for the case of the non-impacting hot streak.

They also conducted these experiments at different density ratios of the streak varying from 0.5 to 1.5 and concluded that there was a relative insensitivity to this. They also concluded that the presence of the stator trailing edge coolant on the rotor does not necessarily lower the hot spot temperatures on the rotor as most of the hot streak is present on the pressure side surface and the accumulation of the coolant is segregated to the suction side surface. This segregation was concluded to be the result of the secondary flows segregating these streams of different densities. But again, most of the measurements were made near the rotor and were not performed for the first stage vane.

1.2.2 Numerical studies

There have been numerous numerical investigations that were carried out to simulate the effects of the hot streak. These studies by Dorney et al. (1990) and Takahashi and Ni (1990) also confirmed the migration of the hot streak towards the pressure side of the rotor. The numerical study by Dorney et al. (1991) predicted that the hot streak does not diminish as it was convected through the stator passage. This study was based on the conditions of the experiments conducted by Butler et al. (1989) which would imply low turbulence levels of the order of 1%. This result did not match up with the experimental results presented in this thesis. But, in general the 2D simulations did not compare well with the experimental results in terms of the prediction of the rotor surface temperatures as they lacked the ability to resolve the secondary flows and also because the flow was not two dimensional in nature.

Dorney et al. (1992) later performed studies to compare both 2D and 3D Navier Stokes simulations. He used a hot streak with a temperature ratio of 1.2 for the conditions of the experiment performed by Butler et al. (1989). Again, this would imply that the numerical study was conducted at low turbulence levels of the order of 1%. The numerical study concluded that in general the 3D simulations matched up better with the experimental results and it was more accurate.

In another numerical simulation performed by Dorney and Gundy Burlet (1996), the effect of clocking the hot streak was studied. Clocking the hot streak refers to the positioning of the hot streak with respect to the vanes. The simulations carried out included both 2D and 3D simulations and concluded that if the hot streak hit the vane, the hot gases are convected with the vane wake and that reduced the temperature load on the rotor. It also indicated that the pressure side of the rotor sees higher temperatures when the hot streak was positioned through the passage. The temperature ratio, which is a ratio of the maximum temperature of the hot streak to the mainstream temperature, varied from 1.10 for the non impacting hot streak to 1.05 for the hot streak impacting the stator vane as measured at the rotor. This result does not agree with the experimental results of Roback and Dring.

Shang and Epstein (1997) also performed 3D simulations to determine the heat loads on the rotor and the physical reasons behind them. Three physical mechanisms were used to explain the rotor blade surface heat load non-uniformity and the overall increase in the heat loads. Buoyancy resulted in driving the high temperature fluid towards the hub and resulting in an increase in the local platform temperatures. The preferential migration of the hot streak to the pressure side increased the local surface temperatures and the temperature non-uniformity.

Unsteady blade row interactions also resulted in the wobbling of the hot streak generating non-uniformities of the total temperature loads on the rotor.

Although the 3D simulations were more successful than the 2D simulations in predicting the flow fields, there is a general lack of experimental data at positions around the vane for comparison to numerical studies under properly described flow field and realistic turbulence levels.

Dorney et al. (1993) performed another numerical simulation that focused on film cooling of a rotor in the presence of a hot streak. This simulation was performed on the rotor pressure surface and both 2D and 3D simulations were carried out. The hot streak temperature ratio used in the 3D simulation was 1.2 and it was introduced through the middle of the passage between the stator vanes. The test case for the 2D simulation had one coolant slot on the pressure surface and coolant at a temperature of 520°R was injected. The density ratio was chosen such that the static pressure at the injection location was equal to the pressure obtained in the absence of film cooling. The mainstream was at 530°R and the hot streak temperature was 636°R . The presence of film cooling reduced the pressure side rotor surface temperatures below the mainstream temperature. Additional cooling slots were added and it was reported that with an increase in the number of cooling slots, the rotor pressure side surface temperatures were further lowered.

For the case of a 3D simulation, two and finally three rows of holes totaling 33 holes, were used and their effects analyzed. As in the case of the 2D simulations, it was found that the presence of three rows of coolant holes, with coolant velocity being 0.4 times the mainstream velocity had eliminated most of the hot temperature spots on the pressure side. It was found that the effectiveness of the coolant increased with an increase in the coolant exit velocity until the effect of the hot streak was nearly completely nullified at a coolant velocity that was 0.4 times the mainstream velocity. It was also concluded in this study that the coolant, simulated at a temperature of 424°R, ejected from the trailing edge of the stator does not affect the temperatures on the pressure side of the rotor as the coolant is mostly segregated on the suction side of the rotor.

The above simulation was the only one that dealt with the effects of both the hot streak and film cooling. The results obtained for the pressure side surface temperatures obtained with film cooling, where the coolant temperatures are only 2% below the mainstream temperature, indicate very high effectiveness levels of the coolant close to 0.9 which does not appear to be very likely. But again, this study was performed on the rotor pressure surface.

The study of hot streaks is completely different for the case of the rotor than the stator vane as the rotor is constantly rotating and thereby chopping the hot streak. In the case of a stator vane which remains stationary, the hot streak can

be positioned at different locations along the pitch which is not possible for the rotor blades.

1.3 OBJECTIVES OF CURRENT STUDY

The foregoing review of previous study of hot streaks shows that there have been no studies, experimental or numerical, that has been conducted on the first stage film cooled vane. There have also been no studies on the effects of the hot streak on the coolant effectiveness for a first stage film cooled vane. The current study focuses on this aspect with a detailed description of the flow field, turbulence levels, and temperature profiles near the leading edge, around the vane and in the wake. One of the primary objectives of this thesis is to find out if the coolant effectiveness can be predicted with the use of an “adjusted” temperature in the presence of a hot streak.

CHAPTER TWO

TEST FACILITY AND EXPERIMENTAL PROCEDURES

2.1 TEST FACILITY

All the tests were conducted in an existing closed loop wind tunnel with a simulated vane model. Modifications were made to the facility to incorporate a heater generator section. Details of the existing facility and the modifications are presented in the following sections.

2.1.1 Mainstream Flow Loop

The wind tunnel consisted of two flow loops, the mainstream flow loop and the coolant flow loop. The main flow loop was powered by a 50-hp fan and the flow was controlled by adjusting the motor speed of the fan. The motor speed was usually set such that the velocity at the inlet to the test section was 5.8 m/s. A schematic of the wind tunnel, shown in Figure 2.1, provides an overall view of the test facility and the mainstream flow loop.

As the test facility used cryogenically cooled coolant jets to obtain a coolant temperature of 250 K required for a density ratio of $DR = 1.2$ with the mainstream temperature at 300 K, the tunnel has to dried out to prevent build up

of moisture in the secondary loop and to prevent the formation of frost on the vane surface. This was done by the use of desiccant packs. These desiccant packs contained a molecular sieve that pulled water and carbon dioxide out of the tunnel air. They were placed in a wooden rack, downstream of the fan, that held seven desiccant packs at about a 20 degree angle to the flow.

Downstream of the desiccant rack, the mainstream flow passed through turning vanes and then flowed through a water flow heat exchanger. Cold water was run through the heat exchanger pipes and fins were provided on the pipe surface to enhance heat transfer. Non-uniformities in the heat exchanger due to clogging of the pipes was a problem when running experiments in the presence of a hot streak as this introduced non-uniformities in the main stream temperature which varied depending on the temperature of the water. This heat exchanger was used to maintain the temperature of the mainstream air at 300 K.

The flow was then turned 90 degrees by the use of turning vanes and then passed through the honeycomb flow straightener and two fine-mesh screens in order to improve flow uniformity and reduce mainstream turbulence. The contraction nozzle then accelerated the flow into the test section. The contraction provided an area reduction of about 4:1. The flow then passed through the heater section of the wind tunnel. At the exit of the heater section, another fine mesh screen was provided to reduce the levels of turbulence and to further make the

flow more uniform. The turbulence generator was positioned at the exit of the heater section. The flow loop then passed through the test section, and decelerated through a diffuser before being returned to the fan.

2.1.2 Secondary Flow Loop

The secondary flow loop refers to the coolant flow loop and was powered by a 7.5 hp centrifugal blower. Air was bled from upstream of the main flow loop fan and was passed through a main heat exchanger and then to a smaller heat exchanger. The second heat exchanger was provided to give better control over the cooling process and to compensate for heating of the coolant flow as it passed through the PVC pipes. Both the heat exchangers were cooled by the use of liquid nitrogen and temperatures were of the order of 160 K. All PVC piping was insulated to reduce heat loss.

From the smaller heat exchanger, the coolant flow was split into three lines to separately feed the suction side, showerhead and the pressure side film cooling holes. The flow was passed through a 1-1/2 inch valve that was used to control the flow and an orifice plate was used to measure the flow rate. The suction side loop was provided with an additional 1-inch needle valve in parallel with the 1-1/2 inch globe valve to provide greater control for the smaller flow rates that are required for one row of holes on the suction side region.

2.1.3 Test Section

The existing test section simulated a linear cascade with the main test airfoil located in the center of the test section as shown in Figure 2.2. Simulated airfoils were placed on either side of the central airfoil, and the flow through the passages on either side of the airfoil was controlled so that a continuous linear cascade was mimicked. The sidewalls and the tailboard were adjustable and were used to equalize the flow in the two passages and to set the stagnation line. The adjustable back walls and tailboard were used to set the pressure distribution around the airfoil. More details on the design and the operation of this test section are provided in Polanka (1999) and Cutbirth (2000).

The surface temperature measurements were made using an infra red camera. As the plexiglass material of the test section does not permit viewing in the infrared region, ports were provided at different locations of the test section. These ports also served as an access panel to the test surface. The port windows were replaced with a NaCl coated salt windows that was used for infrared imaging. Small holes were also drilled on the top of the test section, around the vane and in the wake region, to provide access for a thermocouple rake inserted from the top.

2.1.4 Heater Section

The test facility was modified to install the heater section. The heater section was a 1.17 m long section, with a height of 0.55 m and width of 1.02 m, made to house the movable heater and the flow uniformity rods. It is situated immediately downstream of the nozzle section of the wind tunnel. The design and the construction of the heater section were performed by my fellow researcher Sean Jenkins. The heater was a resistive type duct heater, with 2 different power modes. The heater could be run at full power (7 KW) or at half power (3.5 KW) depending upon the temperature requirement. The heater was held in a square metal duct frame, 200 mm by 200 mm in cross section and 400 mm in length, followed by a 200 mm long transition section leading to a 200 mm diameter circular exit. This translated to a hot streak diameter of $0.44P$, where P is the pitch distance between the vanes.

The heater was held in place by six 27 mm outer diameter hollow rods, which were also used to traverse the heater along the horizontal direction. O-rings were used to seal the tunnel around the rods. To provide uniformity to the flow by providing uniform resistance to the air flow, a number of PVC jam rods were inserted above and below the heater. The number of rods required, rod sizes and their positions were arrived at by trial and error. These were 27 mm outer diameter PVC rods with rubber end grips that were jammed between the two end

walls of the heater section. Two resistance rods of 21 mm outer diameter were also used in the region very close to the heater. The final position of the rods and the heater is shown schematically in Figure 2.3.

A total pressure probe was provided in the heater to detect the flow of air and this acted as a safety mechanism to switch off the heater in the event of no air flow over the heater. The heater cables were brought out through the hollow support rods and connected to an external remote control box. This was then connected to the main power supply through breaker circuits.

The heater was operated at half power under moderate turbulence conditions. Under this mode of operation, the heater provides a temperature ratio of 1.1 at the measurement location of $0.21C$ ahead of the vane, where the temperature ratio was defined as the ratio of the maximum hot streak temperature to the mainstream temperature. For the case of high turbulence, the heater was operated at full power to provide the temperature ratio of 1.1 at the same measurement location.

2.1.5 Turbulence Generator

A passive type turbulence generator was used to obtain the necessary turbulence intensity and integral length scale typical in an operating engine environment. The high turbulence condition was created with an array of rods

located $0.88C$ upstream of the leading edge of the test airfoil. This array consisted of twelve 3.8 cm diameter rods evenly spaced by 8.5 cm across the test section. Further information and verification of the turbulence generator can be obtained from Cutbirth (2000). Turbulence profiles for high and moderate turbulence are provided in Chapter 3.

2.1.6 Test Airfoil

The airfoil geometry was a scaled up version of a commercial turbine vane. The large scale provided a more detailed thermal field resolution. This scaling resulted in a span length of 0.550 m and a chord length of 0.594 m. The Reynolds number was matched to that of real engine operating conditions and based on the exit velocity and the chord length, it was $Re = 1.2 \times 10^6$. The airfoil was made of a low conductivity material of $k = 0.048$ W/mK polyurethane foam with an even wall thickness of 13.7 mm in the front section. The airfoil was divided into three regions, each with a separate plenum, the showerhead, the pressure side and the suction side region. This allowed for separate control of each of these three regions. The showerhead had six rows of cooling holes, the suction side had three rows of cooling holes and the pressure side had two rows of cooling holes. The suction side had a separate hatch section cut out which can be replaced to test different hole geometry and roughness effects.

Figures 2.4 and 2.5 show schematics of the vane and the film cooling configurations. The hole diameter was $d = 4.11$ mm and the spanwise pitch between holes was $P/d = 5.55$. The stagnation line for this airfoil was set on the second row of the showerhead holes counting from the pressure side. Details of the procedure used for setting the stagnation line can be obtained from Cutbirth (2002). A more detailed description of the film cooling hole configurations can be found in Polanka (1999).

2.1.7 Surface Temperature Measurements

An Inframetrics 600L infrared camera was used to obtain the surface temperature measurements. For the measurements on the suction side, the camera was nominally positioned at a distance of 0.28 m from the vane surface. The resolution of the camera is defined as the area over which the camera integrates for a single point measurement. The spatial resolution of this camera is calculated by :

$$Resolution = \frac{Distance}{F * 100} \quad (2.1)$$

where F is the magnification factor. This translated to a spatial resolution of 0.7d by 0.7d in the suction region.

For measurements on the showerhead region, a 3X zoom lens was used on the camera. The camera was positioned at a distance of 0.70 m from the

showerhead surface on the pressure side port. At this location, the spatial resolution of the camera was $0.6d$ by $0.6d$. Video images from the camera were captured on a Macintosh computer using the software, NIH. These images were reduced using a software, Scion Image, a product of Scion Corporation. The data reduction process was done over a four by four pixel block. Each pixel as obtained from Scion Image corresponded to an area of $0.06d$ by $0.06d$. This resulted in a final resolution of the camera of $0.8d$ by $0.8d$.

2.1.8 Thermocouple Rakes

Two different thermocouple rakes were used in these experiments. One rake was used to measure the hot streak and the other one was used to measure the temperature field close to the wall. The rake used for measuring the hot streak had six E type thermocouples spaced uniformly at 36 mm. The thermocouples were made out of 0.6 mm diameter thermocouple wires with a 0.4 mm thick insulation that was stripped at the edge. The rake had a flexible arm, with a support rod/prong for each thermocouple.

As the thermal field near the vane required a different resolution to capture the details of the coolant next to the vane, a different rake was used. This rake also used six E type thermocouples made out of same 0.6 mm diameter thermocouple wires. The thermocouples were spaced such that they were closer

near the vane surface. For this reason, the first three thermocouples were spaced 2 mm apart while the next three thermocouples were spaced at 5 mm from each other.

2.2 EXPERIMENTAL PROCEDURE

2.2.1 Velocity Measurements

All velocity measurements were made by the use of a 3.2 mm diameter Pitot-static probe. The probe was inserted from the top of the tunnel for the vertical profile measurements, and a manually controlled traverse was used to move the fixture holding the probe. The probe was connected to a Validyne DP103 differential pressure transducer and values were recorded from the digital display. The Validyne was accurate to within 0.5% of its full scale of 86 Pa. The traverse was usually moved in increments of 12.5 mm. Knowing the pressure, and the density of air based on the temperature at that location, the velocity was calculated using the Bernoulli equation. Vertical and horizontal profiles of the streamwise velocity are presented in Chapter Three.

2.2.2 Turbulence measurements

To perform turbulence measurements, a single sensor hot-wire anemometer, which had a platinum coated tungsten wire, was used. These

measurements were also made at a location $0.21C$ upstream of the leading edge. The hot-wire probe was again traversed in the vertical or spanwise direction by the use of a traverse, and the voltages were acquired through an AMUX-64 data acquisition board and were read using the LabVIEW program. A more detailed description of the data acquisition equipment is provided in Polanka (1999). The hot-wire anemometer was calibrated by measuring the velocity at the same location as the hot wire probe using a Pitot-static probe. A fourth order polynomial curve fit was then used as a calibration curve.

The mean velocity and the rms velocity were calculated using a sample size of 4000 data points averaged over a four second time period. The integral length scales were estimated from the integral time scales using Taylor's hypothesis that were determined from autocorrelations of the data points.

2.2.3 Adiabatic Effectiveness Tests

The adiabatic effectiveness experiments were performed in the showerhead region and following the first row of holes on the suction side. These experiments were performed with and without a hot streak to evaluate the effect of the hot streak on the coolant effectiveness. The tests were run at a density ratio of 1.2 and were conducted for a range of blowing ratios varying from 0.5 to 2.0. The first step was to dry out the tunnel air. To achieve this, the desiccant packs

were put in the furnace overnight or for a period of four hours to remove all the moisture already present in them. They were then placed back in the rack and the tunnel was run for one to two hours. The blower was also switched on at intervals to dry out the coolant loop as well. A digital hygrometer was placed near the coolant holes to measure the humidity of the tunnel as well as the secondary flow loop. As the tests were run at a density ratio of 1.2, the humidity in the tunnel did not pose a big trouble in running the experiments. A relative humidity value less than 10% was considered to be dry enough to run these experiments.

The hot streak temperatures were then measured. To do this, the mainstream was first set such that the velocity in the test section was 5.8 m/s. The heater was then turned on and a thermocouple rake was inserted from the top of the tunnel. The heater was then allowed to reach its full operational capacity and this usually took a couple of minutes. The rake was then traversed and temperatures were measured at various streamwise and spanwise locations near the vane region under study.

Once the hot streak profile had been mapped around the vane region under inspection, the thermocouple rake was removed and the cooling process was started. The rake had to be removed to prevent disturbances to the flow field that would have affected the measurements. The blower was then turned on and the required blowing ratio was set. The pressure drop across the orifice meter present

in the coolant flow loop was measured, and this in turn was used to calculate the flow rate in the secondary loop. The pressure drop was measured by the use of a Validyne pressure transducer and the values were read out from the digital display. The main heat exchanger was first cooled down using liquid nitrogen. The nitrogen tank connected to the smaller film cooling heat exchanger was then turned on. Thermocouples were placed in both the heat exchangers to monitor the temperatures.

Two type E ribbon type thermocouples were placed on the inside surface of the vane on the suction side and one thermocouple was placed in the showerhead region. These temperatures were monitored and the cooling process was continued slowly until the required coolant temperature (250K) was reached. This process usually took a couple of hours. If the process was not carried out slowly, it was very difficult to get the system to reach a steady state.

Once a steady state had been reached, images were then recorded using the infrared camera, with the video looped to a Macintosh computer. The images were averaged over 60 frames. The temperature values were also averaged over the same time span of 10 seconds using the LabVIEW program. The flow rate was then adjusted for a different blowing ratio and the whole process was repeated for a variety of blowing ratios. At each blowing ratio, the system was allowed to reach steady state. After the effectiveness measurements were

completed, the heater was then turned on and the entire process was repeated in the presence of a hot streak. Also, to ensure repeatability within a test, a particular blowing ratio was repeated again towards the end of the experiment. Usually, on the suction side region, measurements were made for a blowing ratio of $M = 1.0$ and on the showerhead region, measurements were made for $M^* = 1.4$ at the beginning and at the end of the experiment.

After the completion of the effectiveness tests, the thermocouple rake was again inserted and temperature profiles were measured at specific location with just the coolant blowing and for the conditions of the coolant with the hot streak. These measurements were done for two different blowing ratios.

The last part of the experiment was the calibration of the camera. To do this, a 60 mm by 40 mm copper plate was stuck to the vane surface with two type E thermocouples stuck on to the plate. The plate was painted black to match the vane surface. The use of a copper plate with its high thermal conductivity helped eliminate sharp temperature gradients and provided a more uniform temperature. This meant that small errors in the measurement of the position of the thermocouples did not result in bad calibrations. The plate was cooled in a controlled manner by the use of nitrogen jet. Images averaged over 10 frames along with temperature readings were saved every couple of degrees. The thermocouple locations were then marked by the use of a hot pointer. The last part

of the experiment was to account for the curvature of the vane surface as seen by the camera. A piece of ruled tape was stuck on the vane surface and images were taken with a hot pointer at every centimeter. The entire experiment lasted for about 10 hours.

2.2.4 Hot streak measurements

Hot streak measurements were made using the evenly spaced thermocouple rake inserted in the tunnel from the top. The hot streak generator was switched on and the coolant water was turned on to maintain the tunnel at 300K. The rake was then traversed to the middle of the tunnel near the center of the hot streak and rotated along the z -axis until the maximum temperature was measured by the third thermocouple. This ensured that we covered the entire range of temperatures on either side of the maximum temperature. The rake was again moved back to the top of the tunnel and the temperatures were recorded by averaging over 10 seconds using the LabVIEW program. The rake was traversed in increments of 12.5 mm by the use of a manually controlled traverse and temperatures measurements were recorded along with the mainstream temperature. The locations of the thermocouples were measured by measuring their distance from the sidewall.

2.3 DATA REDUCTION PROCESS

The data images were reduced by the use of the software, Scion Image a product Scion Corporation. A separate macro for calibration was used to obtain the grayscale values averaged over a 4 x 4 pixel block at the location of the thermocouples. These grayscale values were then plotted along with the temperature values that were recorded for the images. A calibration curve was then generated by fitting a curve through these data points. A third or sixth order curve was generally used for this purpose. A sample calibration curve is provided in Figure 2.6.

The image files that were recorded for the different blowing ratios were then reduced to grayscale values. To do this, an area of the image covering three holes was considered and grayscale values were average for a 4 by 4 pixel region. There was a total of 5050 points that were obtained from this process. The data was represented with an x location, a z location and the average grayscale value.

These values were then transported to Excel. The grayscale values were then converted to temperature values by using the calibration curve. The x and z pixel values were converted in terms of x/d and z/d values. To transform the x pixels into x/d values, the earlier recorded values of the streamwise distance was used to generate a plot between x pixel location and x/d and a curve was then fit

through the data points. The equation of the curve was then used to convert all x pixel values into x/d values.

For converting z pixels into z/d values, the fact that the distance between the camera and the airfoil was constantly varying had to be taken into account. This difference resulted in images displaying the jets being turned. To straighten the jet, around 10 points were taken along the centerline of the top and bottom jet. The physical distance between two adjacent holes is known to be $5.55d$ and using the center of the bottom jet as 0 and the center of the top jet as $11.1d$, the data was adjusted to account for the change in viewing distance. The use of a curve to fit these data points was again used to transform the z pixels into z/d values.

The next step in the process was to account for the error due to conduction, as the surface was not truly adiabatic. To incorporate a 1D conduction correction, the fact that at the highest blowing ratio of $M = 1.4$ in the suction side region, the jet lifted off the surface was used. The jet had little or no effect midpitch between the coolant holes. Line scans were thus done at midpitch of the coolant holes, and these were converted to an effectiveness value (η_0). This value was then used for all blowing ratios as the error in conduction. Ethridge et al. (1999) determined that internal heat transfer coefficient had a negligible effect on conduction correction, and therefore conduction correction was independent of

blowing ratio. The corrected effectiveness values were calculated based on the following formula

$$\eta_{corr} = \frac{\eta - \eta_0}{1 - \eta_0} \quad (2.2)$$

A more detailed explanation of the 1D conduction errors and the correction factor can be obtained from Cutbirth (2000).

The laterally averaged effectiveness was then calculated by averaging all the effectiveness values between two hole pitches measured from the first jet centerline to the third jet centerline for each x/d location. This was earlier done using an Excel macro. Later, MatLab was used to generate a 100 by 100 grid of effectiveness values in the region of two hole pitches and then effectiveness was calculated by averaging the effectiveness at different z/d locations for each x/d value. Contour plots of the local effectiveness values were then plotted for the different blowing ratios by the use of Deltagraph.

2.4 UNCERTAINTY ANALYSIS

2.4.1 Effectiveness Tests

The uncertainty in measurement of the temperatures affected the values of the effectiveness of the coolant. The uncertainty in the surface measurement of the temperature was based primarily on the calibration of the infrared camera and the spatial resolution. Once data was recorded for the values of grayscale and

temperature, a calibration curve was produced by fitting a curve through the data points. The temperature values were recalculated using the calibration curve and compared against the observed temperatures. The standard deviation was calculated using the following formula

$$\sigma = \sqrt{\sum_{j=1}^N \frac{(T_{meas} - T_{calc})_i^2}{N - (m + 1)}}$$

where N is the number of thermocouple measurements, and m is the order of fit of the calibration curve. The value of N was usually around 50 and the order of fit, m, was usually five.

Different thermocouples were placed at various positions in the test section to measure the mainstream temperature and to account for the variations in the mainstream temperature across the test section. Based on these measurements and the measurements of the mainstream temperatures recorded during the experiments, an uncertainty value was obtained to be $\delta T_{\infty})_{prec} = 0.4$ K. The bias errors between the thermocouple, detected by the use of a constant temperature source ice bath, were found to be $\delta T_{\infty})_{bias} = 0.2$ K.

The total uncertainty in measuring the effectiveness was calculated by using the sequential perturbation method where the effectiveness values obtained by perturbing each of temperature variables by their uncertainty in measurements was used to calculate the total uncertainty of the measurement. The effectiveness

values obtained for the repeatability test blowing ratios were also analyzed to obtain the total uncertainty.

For the measurements on the showerhead region, the uncertainty in measuring the surface thermal measurements was $\delta T_{aw} = \pm 1.7 \text{ K}$. Using this value of uncertainty, the total uncertainty in measuring the effectiveness was $\delta \eta = 0.05$. For the measurements on the suction side, the surface temperature uncertainty was $\delta T_{aw} = \pm 1 \text{ K}$. The uncertainty in the effectiveness values as calculated using these uncertainty measurements was $\delta \eta = 0.03$.

The spatial resolution of the camera, which varied between $0.6d$ and $0.7d$, meant that the camera provided one single value average over an area of $0.6d$ by $0.6d$. But, for the data reduction process, these values were averaged over a 4 by 4 pixel block and the final resolution was $0.8d$ by $0.8d$. Scion image then averaged the temperatures in this block and provided a single temperature value for this area.

2.4.2 Hot Streak Measurements

For the hot streak measurements, the uncertainty of the temperature ratio was calculated in the same manner as before. Repeated temperature measurements were taken for the hot streak temperature using a thermocouple over a three minute period and these measurements were repeated again after 30

minutes. Each measurement value was based on a 10 second average. Based on these temperature values, the error in the measurement of the hot streak temperature was found to be, $2\sigma = 0.4$ K. This resulted in an uncertainty in the temperature ratio $\delta(T/T_\infty)$ of ± 0.002 .

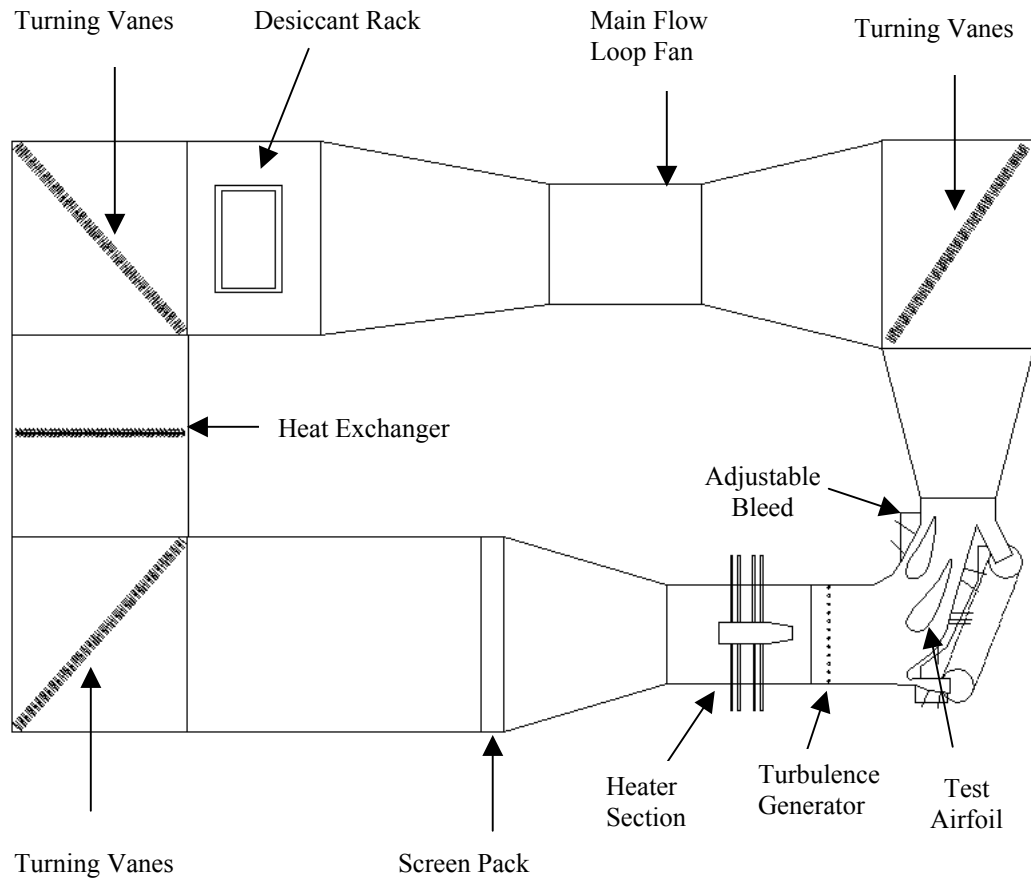


Figure 2.1 : Schematic of wind tunnel

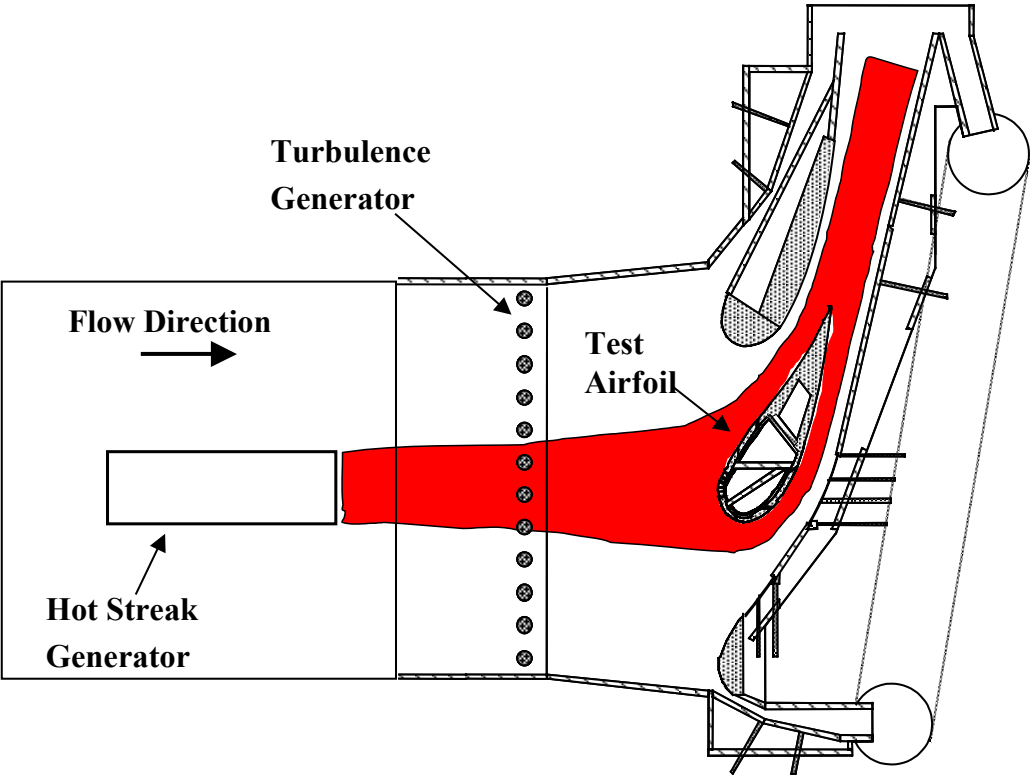


Figure 2.2 : Schematic of test section and the hot streak generator (Jenkins et al. (2003))

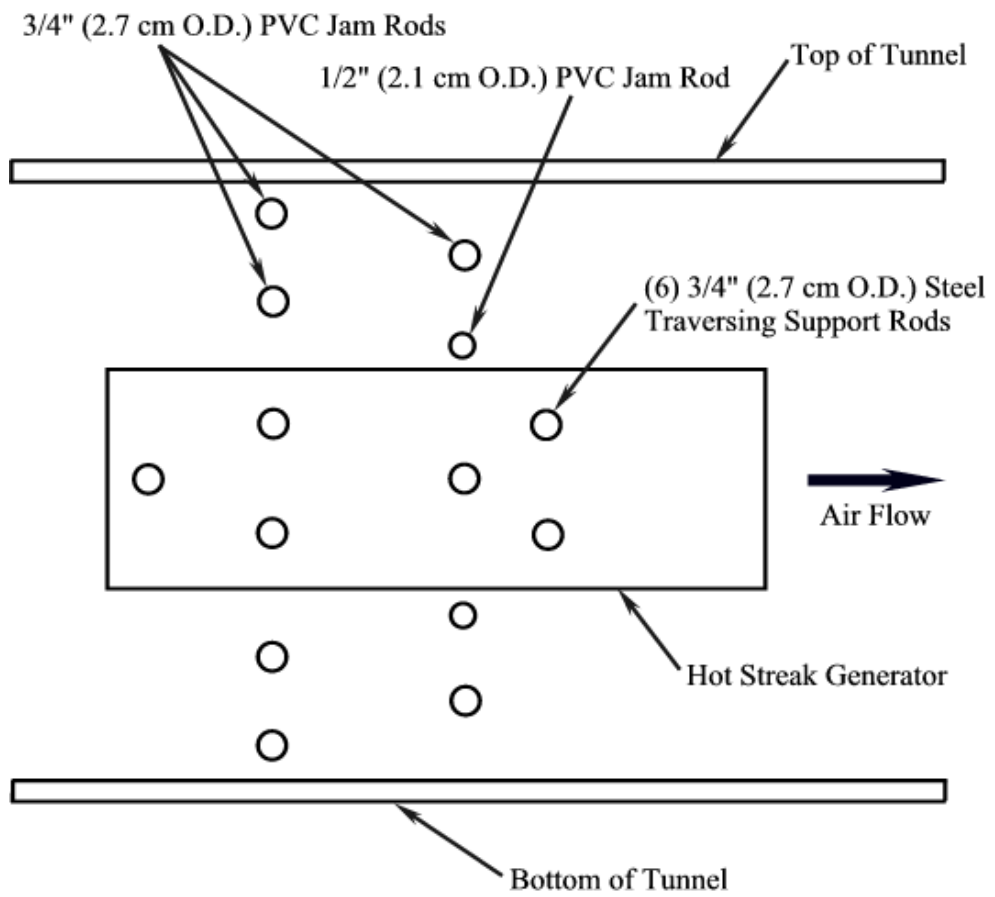


Figure 2.3 : Positions and sizes of the support rods and the resistance rods in the hot streak generator section. (Jenkins et al. (2003))

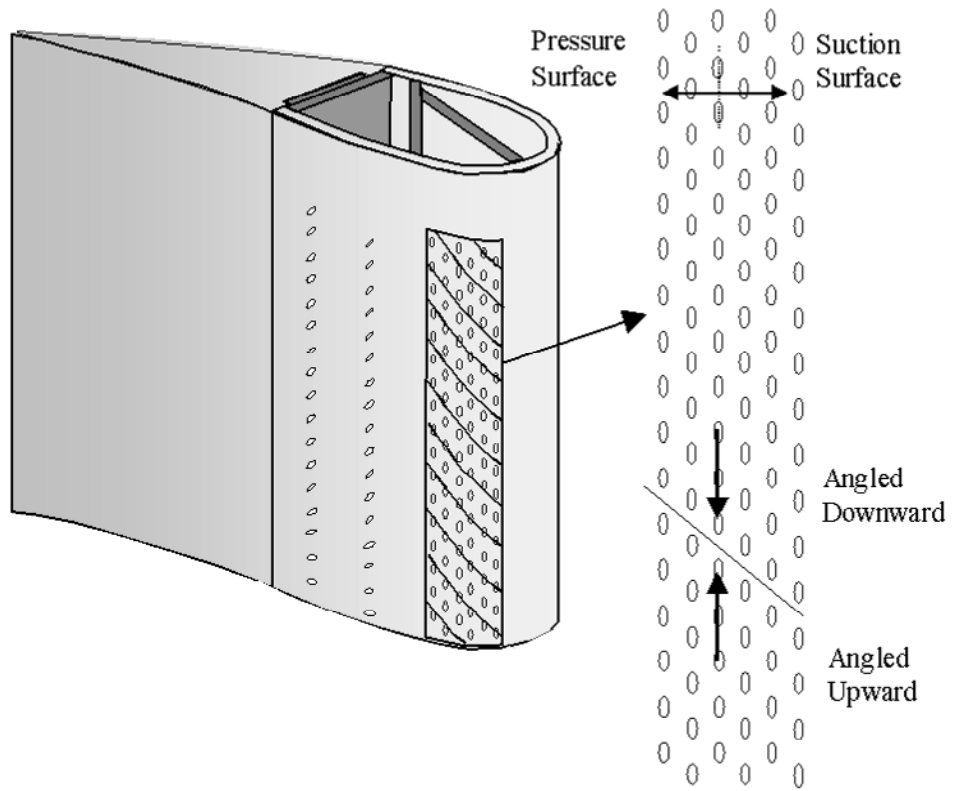


Figure 2.4 : Test Vane with showerhead and pressure side film cooling holes

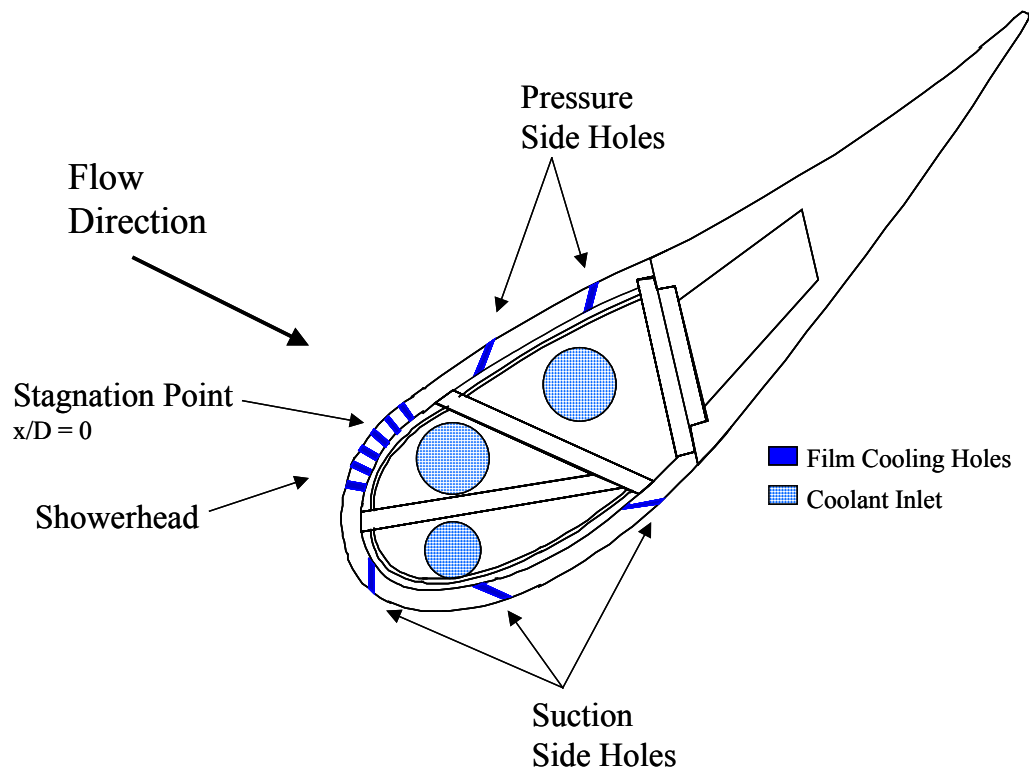


Figure 2.5 : Schematic of Film cooling hole configurations

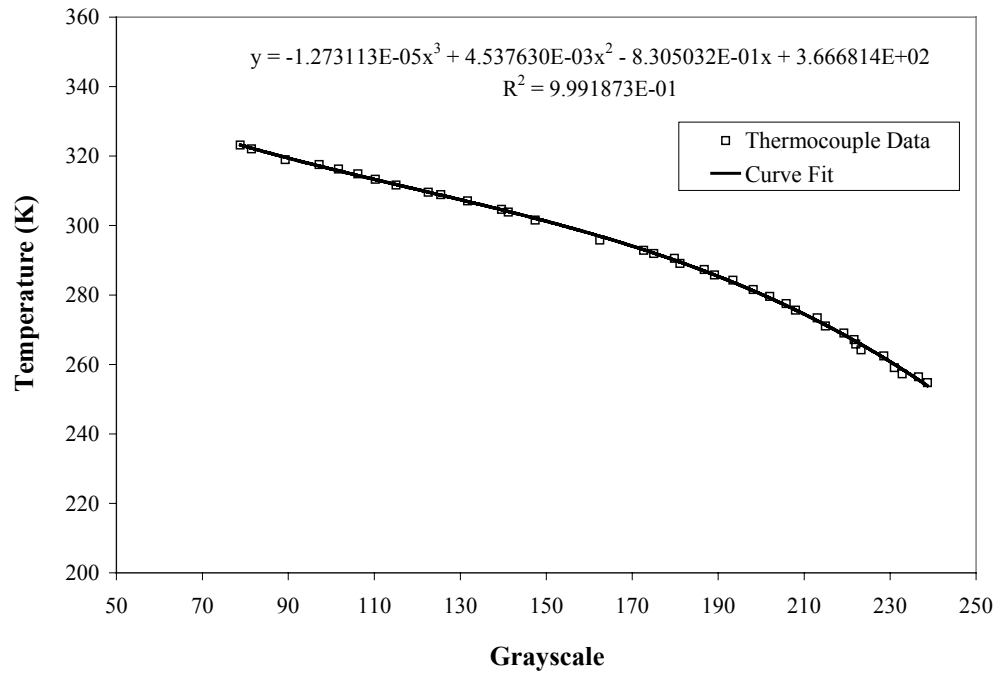


Figure 2.6 : Sample Calibration Curve

CHAPTER THREE

FLOWFIELD CONDITIONS AND HOT STREAK MEASUREMENTS

3.1 FLOW FIELD MEASUREMENTS

3.1.1 Velocity Measurements

Velocity measurements were measured at a location $0.14C$ upstream of the leading edge across the test section in the horizontal direction. The flow across a linear cascade of turbine should be periodic and a proper simulation of a cascade requires us to have a periodic flow. As the flow approaches the vane, the flow accelerates upstream of the turbine passage and slows down approaching the leading edge of the vane. To determine the uniformity in the flow, the relative level of the peaks and troughs was compared. The tail board was adjusted to adjust the flow through the passages and obtain this uniform flow. The final velocity measurements shown in Figure 3.1 indicate that the two peaks and the three troughs were within 2% of each other assuring us of a periodic flow. These measurements also compare well with the measurements made by Cutbirth (2000) at the same location.

Vertical profiles of the streamwise velocity were also measured to ensure the uniformity of the flow field entering the test section. Velocity measurements were made near the vane at $0.21C$ upstream of the leading edge. This location had been used in all previous studies in this facility to describe the flow field conditions and choosing this location provided us with a baseline comparison against earlier measurements. The velocities were measured using a Pitot-static probe traversed using a manually controlled vertical traverse.

Velocity profiles were measured across the heater and across the resistance rods and are shown in Figure 3.2 for moderate turbulence conditions. The use of the resistance rods to provide a uniform flow resistance and the use of a fine screen mesh provided more uniformity to the flow as seen in the figure. The measurements showed that the mean velocity profiles were uniform within $\pm 3\%$.

Similar measurements were also made under high turbulence conditions. These measurements are plotted on Figure 3.3. Under these conditions as well, the flow was uniform as in the case of moderate turbulence the mean velocity profiles were uniform within $\pm 2\%$ for the region measured.

Velocity measurements were also made with the heater turned on. As the total pressure is a constant value, with heating of the air there is an increase in the density of the air proportional to the increase in the temperature values. This results in an increase in the velocity proportional to the square root of the density

and this was confirmed by our measurements. Figure 3.4 shows the plots of the velocity ratio with and without the hot streak generator activated to highlight this difference. The difference in the velocities is proportional to the change in temperature as related by $(T_{hs}/T_{\infty})^{1/2}$.

3.1.2 Turbulence Measurements

All turbulence measurements were made with the use of a hot wire anemometer and were performed at the same location as that of the velocity measurements which was $0.21C$ upstream of the leading edge of the vane. Turbulence intensities along with the length scales were measured in the spanwise direction using a vertical traverse. These measurements were also made downstream of the resistance rods and downstream of the centerline of the hot streak generator.

The turbulence levels for the moderate turbulence conditions are shown in Figure 3.5. For the moderate turbulence condition, the level of turbulence varied across the resistance rods and across the heater. The turbulence levels over the resistance rods were nominally $Tu = 5\%$ with an integral length scale of $\lambda_f = 32$ mm, with slight variations in the spanwise direction. Similar turbulence intensity and length scales were found above the hot streak generator. However, at a

position coincident with the center of the hot streak the turbulence intensity was $Tu = 2.5\%$ with an integral length scale of $\Lambda_f = 18$ mm.

However, under high turbulence conditions, the turbulence levels were more uniform. With the turbulence generator in place, the turbulence intensity was nominally $Tu = 20\%$ and integral length scale was nominally $\Lambda_f = 32$ mm. These values are plotted in Figure 3.6 and the values are similar to the earlier measurements made in this facility by Cutbirth (2002). This indicates that the turbulence levels created by the turbulence rods overwhelm the turbulence generated by the presence of the hot streak generator. The length scales normalized by the pitch distance between the vanes (P) was $\Lambda_f/P = 0.07$. These levels are similar to levels found in actual engines as reported by Radomsky and Thole (1998).

3.2 HOT STREAK MEASUREMENTS

The hot streak measurements made at a distance of $0.21C$ upstream of the leading edge were used as the reference hot streak measurement location. These measurements were made with the hot streak passing through the mid passage. Measurements were made using the thermocouple rake under both moderate and high turbulence conditions. Measurements were also made in the wake region which was $0.32C$ downstream of the trailing edge to study the attenuation of the

hot streak under the effect of mainstream turbulence. The tunnel temperature was also measured each time and the hot streak temperature ratio (T/T_∞) was used to represent the temperature at all locations. In certain cases, it was found that a better comparison could be made by the use of a normalized temperature ratio Θ_R , defined as

$$\Theta_R = \frac{T_{hs} - T_\infty}{T_{0,hs} - T_\infty}$$

where T_{hs} was hot streak temperature at a point in the flow and $T_{0,hs}$ was the upstream peak hot streak temperature at the reference location

The normalized mean temperature profiles measured at the reference location of 0.21C upstream of the leading edge are shown in Figure 3.7 for moderate turbulence along with measurements in the wake region at 0.32C downstream of the trailing edge. Similar profiles are plotted in Figure 3.8 for the high turbulence condition. At the reference location, the value of $\Theta_R = 1$ because of its definition. As the hot streak passes through the passage, the hot streak is attenuated by the effect of turbulence and the measurements taken in the wake region show this drop in the hot streak temperature.

As can be seen from the two figures, the hot streak profile for the high turbulence case is much broader than the profile of the moderate turbulence case. This is expected due to the increased dispersion caused by high turbulence. Also,

the figures show a larger attenuation for the high turbulence case. The Θ_R value in the wake region is 0.44 for the high turbulence case as compared to 0.54 for the moderate turbulence case. This corresponds to a 20% difference in the peak Θ_R values as measured in the wake between the two cases.

A complete 2D profile was taken in the wake under these conditions and the contour plots are shown in Figure 3.9. In this figure $y/P = 0$ corresponds to a streamline originating from the trailing edge of the vane, with negative and positive y/P values corresponding to the suction side and pressure side of the test vane, respectively. Furthermore, $y/P = \pm 0.2$ correspond to the wall and vane on either side of the test vane

Two points that are immediately noticeable are the narrowing of the hot streak as compared to the reference location and the spreading of the hot streak in the z direction. As the hot streak passes through the tunnel passage, the area of the passage is reduced by a factor of 5. This can be seen from the schematic of the test section shown in Figure 2.2. This results in the hot streak being squeezed in the y direction and spreading more in the z direction. Also visible in the plots is the larger amount of spreading in the case of high turbulence. This is an important factor as the larger spread of the hot streak for the high turbulence case resulted in much smaller gradients.

3.3 EFFECT OF THE VANE ON THE HOT STREAK

Experiments were also performed to evaluate the effect of the vane on the hot streak. The hot streak generator was moved such that the hot streak impacted on the stagnation line of the vane. Temperature measurements were made at the reference location and in the wake. These measurements were compared with the measurements made with the measurements in the wake for the hot streak passing through the middle of the passage.

Figure 3.10 shows a plot of the normalized temperature profiles measured in the wake for the impacting and the non-impacting hot streak. It is evident from these figures that the profiles for both the impacting and the non-impacting hot streak were very similar. The peak value with the hot streak impacting the stagnation point was $\Theta_R = 0.46$ with a slightly lower value of $\Theta_R = 0.44$ for the non-impacting case. But, from these plots, we also see that there is a larger spreading of the hot streak when it is centered through the passage and a decreased dispersion for the impacting hot streak. As the mainstream turbulence is large scale turbulence, with $\lambda_f = 32\text{mm}$, the turbulence close to the vane surface, within about 30mm ($0.07P$), will be suppressed by the presence of the vane. This may account for a more coherent hot streak following its impact with the vane.

Further measurements of the impacting hot streak were made as it passed around the vane under high turbulence conditions. A complete 2D profile of the

hot streak was also made at the reference location. These measurements were made at one third and two thirds of the total distance along the suction and pressure sides and are represented in Figure 3.11 and Figure 3.12. From the figures, the contraction of the hot streak along the suction side is clearly visible. This results in sharper gradients being present near the wall in the suction side region. There was a significant attenuation of the hot streak in the first one third of the distance along the suction side. The hot streak temperature ratio had dropped to $T/T_\infty = 1.061$ in this distance. It dropped further to $T/T_\infty = 1.052$ by the time it got around two thirds of the distance on the suction side. The temperature ratio in the wake was $T/T_\infty = 1.048$ as compared to $T/T_\infty = 1.102$ at the reference location.

The rate of attenuation of the hot streak on the pressure side was very different compared to the suction side. The hot streak temperature had only reduced to $T/T_\infty = 1.081$ in the first one-third distance as compared to $T/T_\infty = 1.061$ for the suction side. Also the hot streak was much wider on the pressure side. This can be attributed to the fact that the streamlines on the suction side converge more than those on the pressure side resulting in squeezing in the hot streak on the suction side.

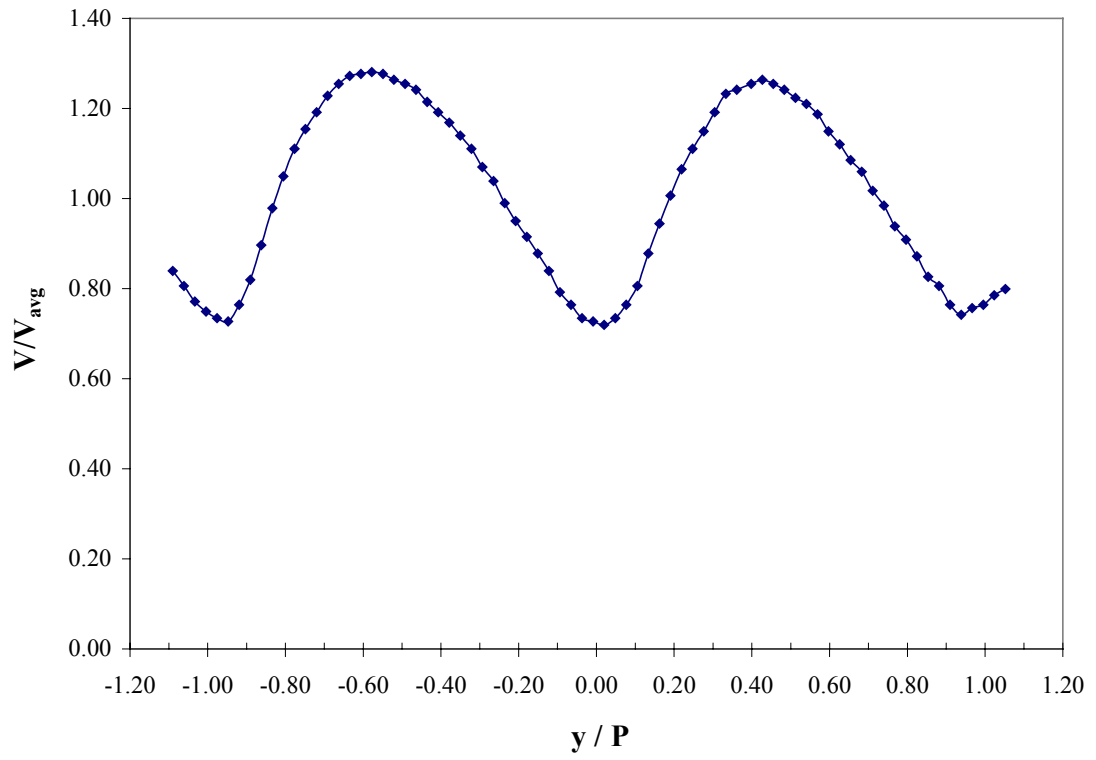


Figure 3.1 : Horizontal profile of the streamwise velocity measured at 0.14C upstream of the leading edge.

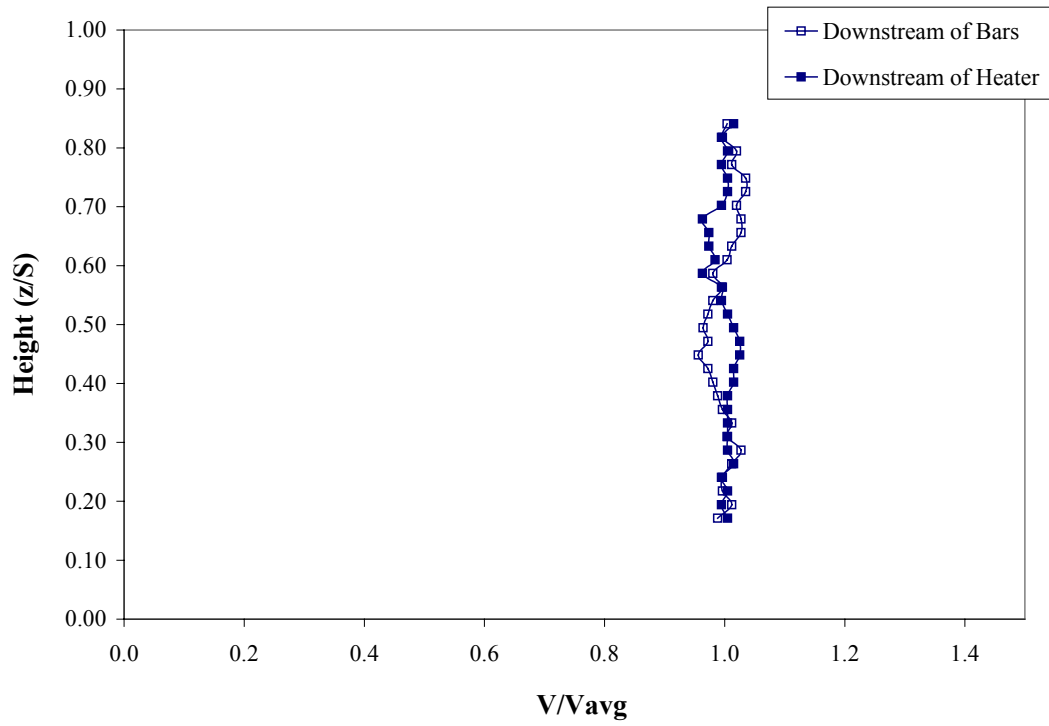


Figure 3.2 : Vertical profile of the normalized velocity distribution measured at $0.21C$ upstream of the leading edge under moderate turbulence levels.

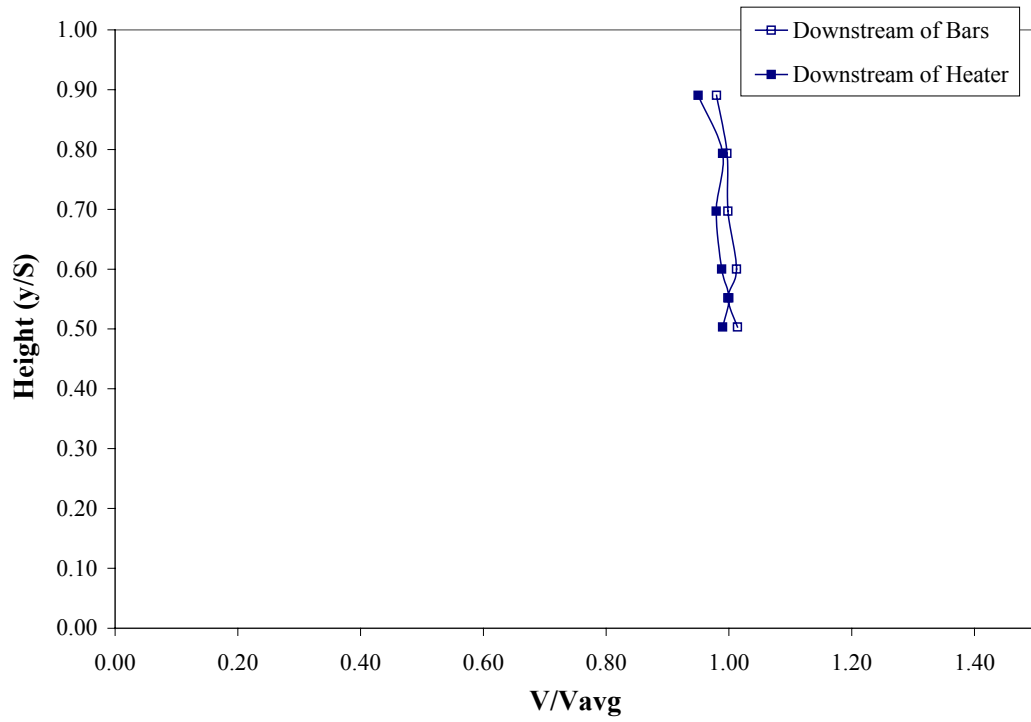


Figure 3.3 : Vertical profile of the normalized velocity distribution measured at $0.21C$ upstream of the leading edge under high turbulence levels.

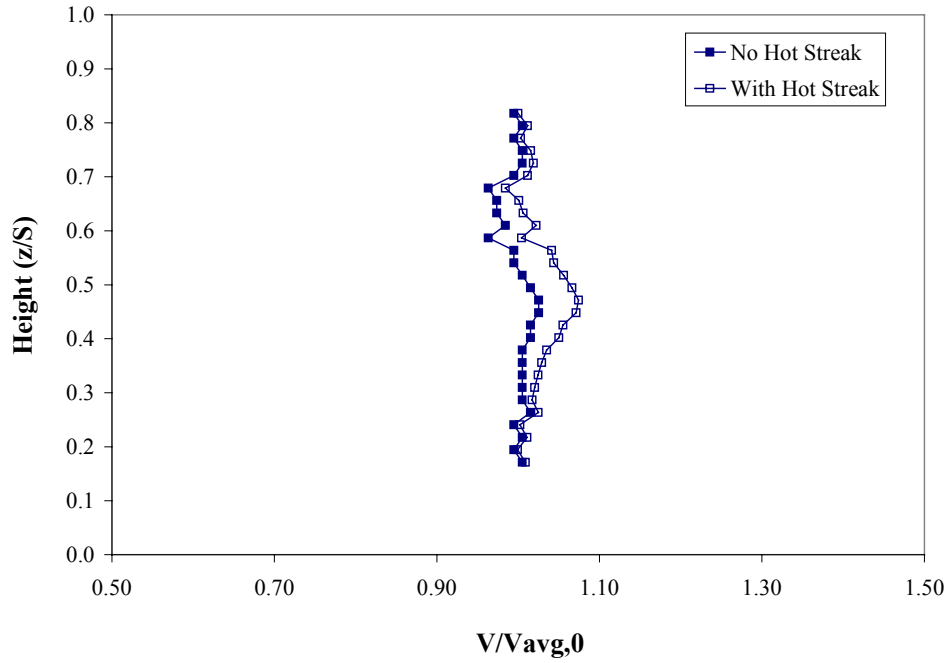


Figure 3.4 : Vertical profile of the normalized velocity measurements made at a location 0.21C upstream of the leading edge across the heater under moderate turbulence with and without the hot streak.

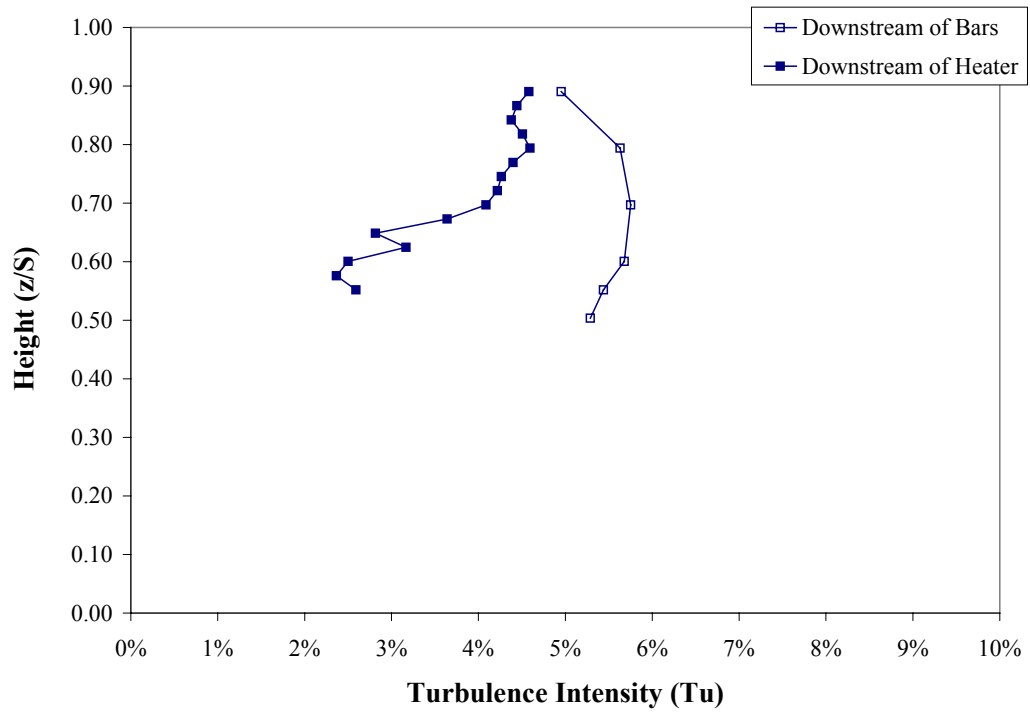


Figure 3.5 : Turbulence measurements made at a location $0.21C$ upstream of the leading edge under moderate turbulence conditions.

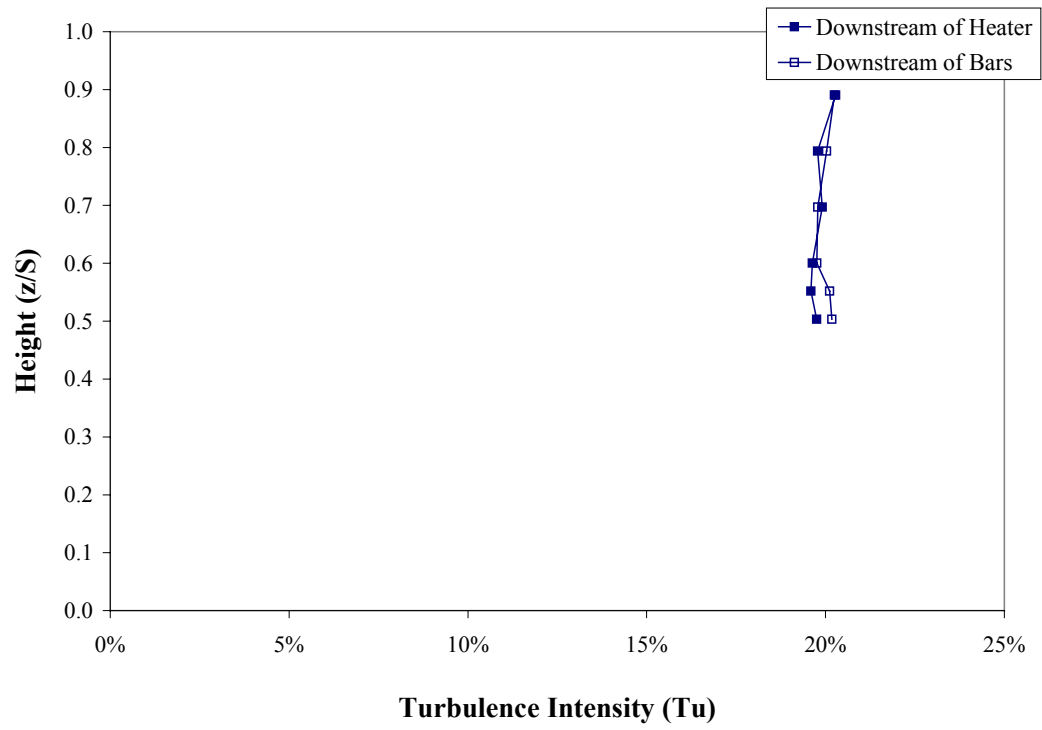


Figure 3.6 : Turbulence measurements made at a location $0.21C$ upstream of the leading edge under high turbulence conditions.

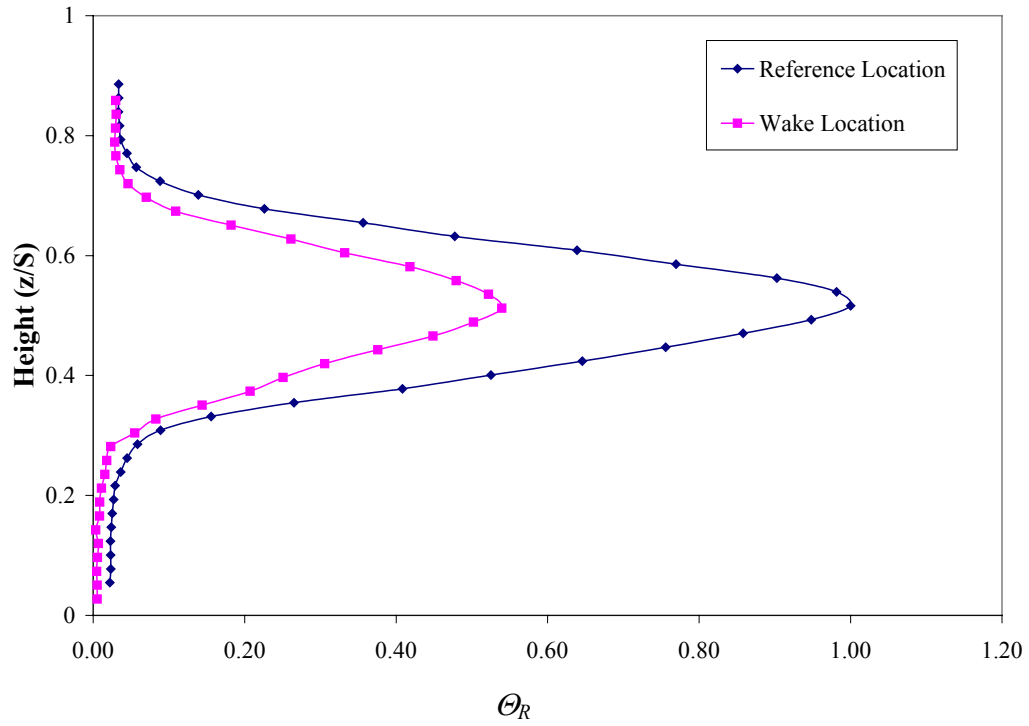


Figure 3.7 : Normalized temperature profiles measured at the reference and wake location under moderate turbulence.

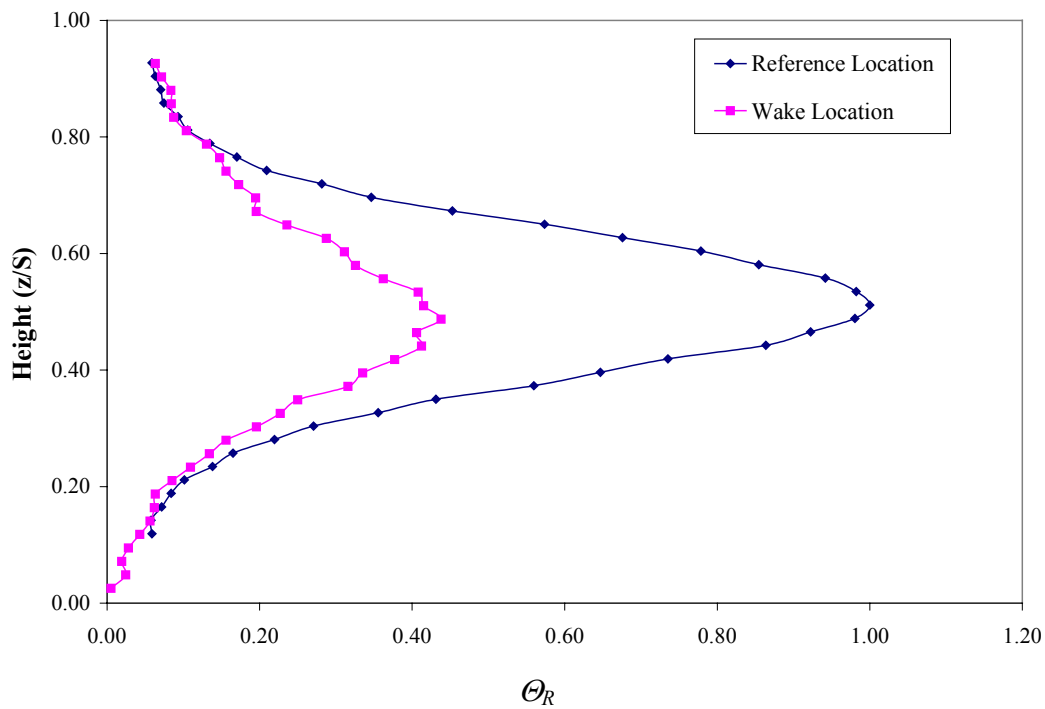


Figure 3.8 : Normalized temperature profiles measured at the reference and wake location under moderate turbulence.

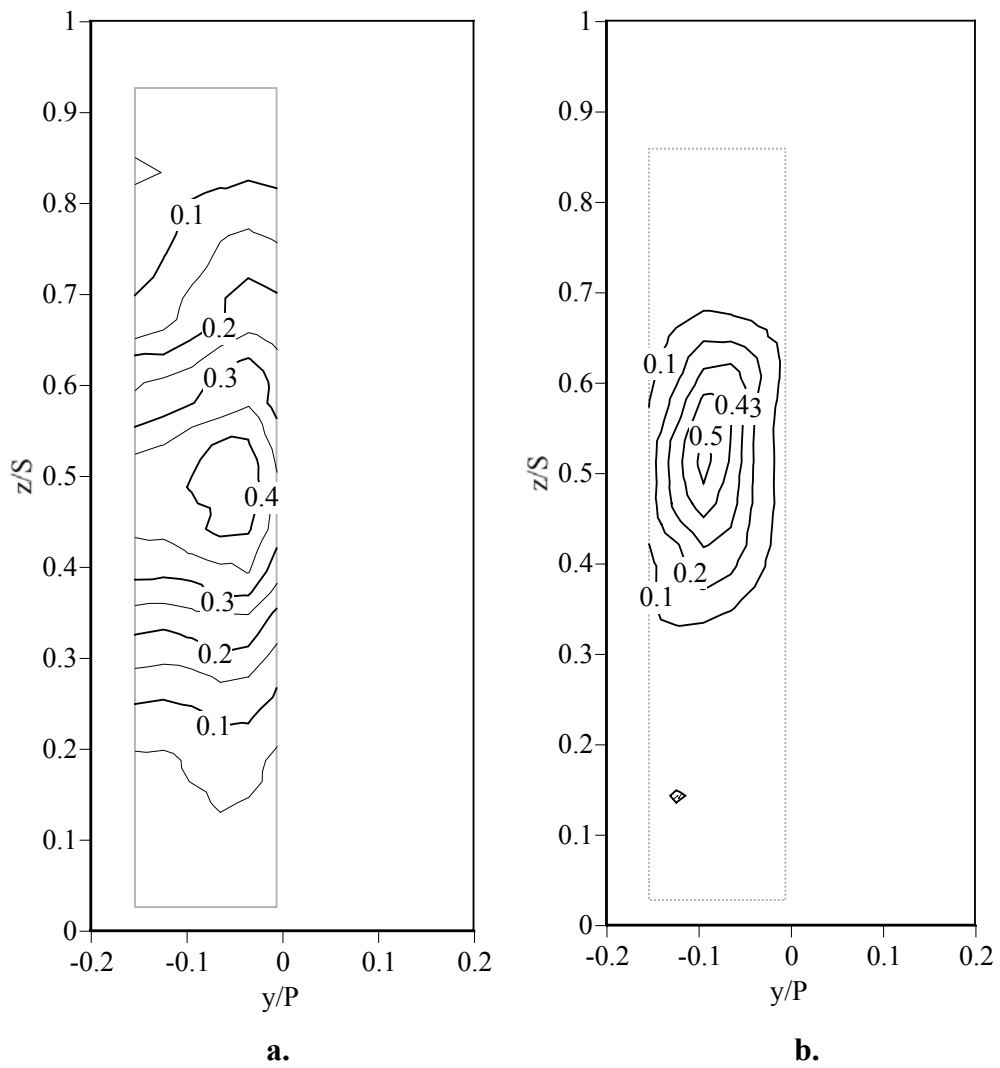


Figure 3.9: Normalized temperature ratio plot in the wake at a location 0.32C from the trailing edge for the hot streak aimed through the passage

- a. High Turbulence**
- b. Moderate Turbulence**

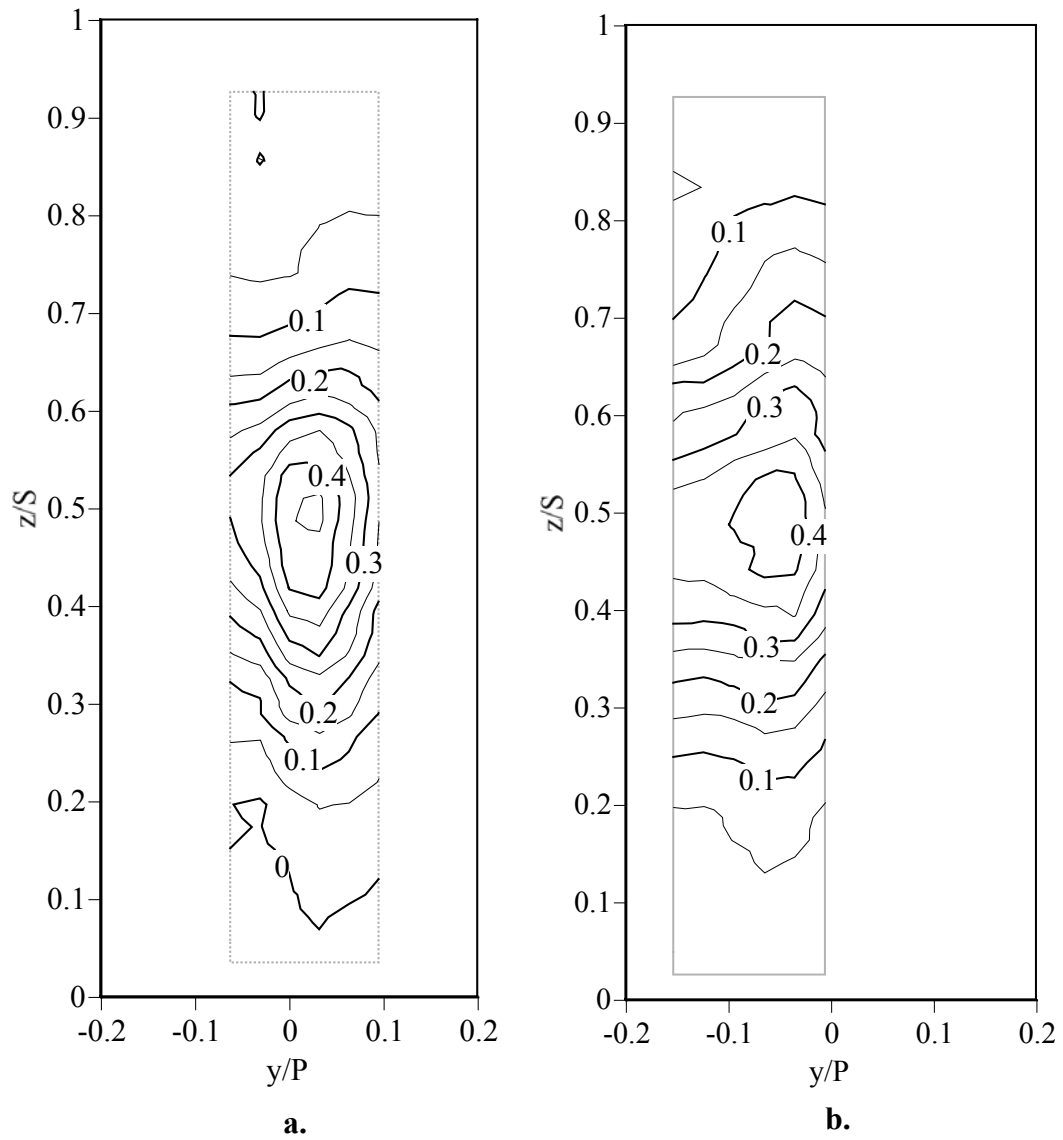


Figure 3.10: Normalized Temperature ratio plot measured in the wake at a location 0.32C from the leading edge under high turbulence

- a. Hot streak on the stagnation line**
- b. Hot streak through the passage**

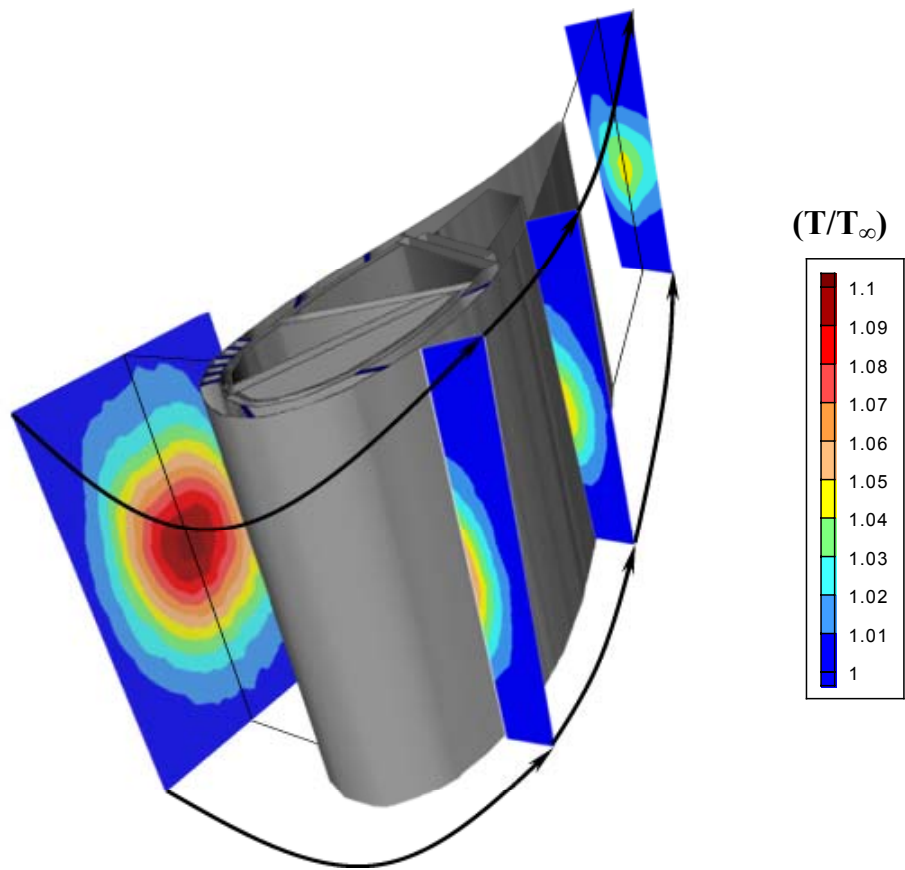


Figure 3.11 : Temperature profiles measured along the suction side with the hot streak impacting the vane (Jenkins et al. (2003)).

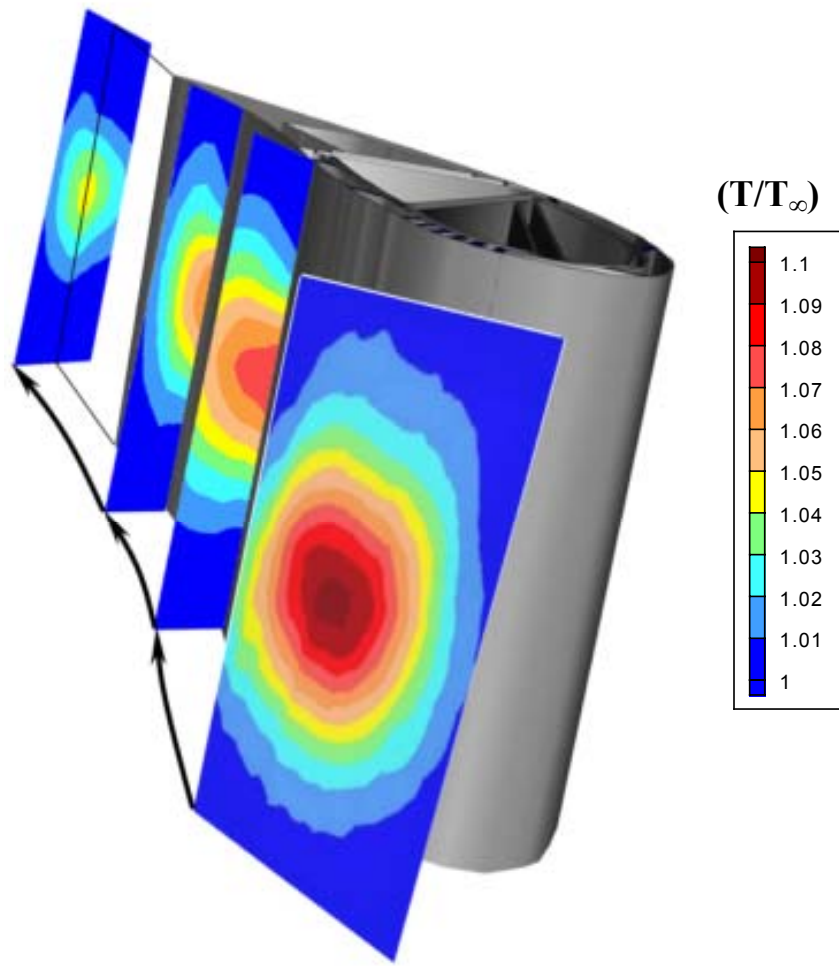


Figure 3.12 : Temperature profiles measured along the pressure side with the hot streak impacting the vane (Jenkins et al. (2003)).

CHAPTER FOUR

EXPERIMENTAL RESULTS

One of the objectives of this thesis was to determine the effect of a hot streak on the film cooling performance and to verify if the use of an adjusted mainstream temperature measured at some location near the wall would scale the adiabatic effectiveness levels to the values obtained without a hot streak. The test conditions are explained in more detail in Section 4.1. The experimental results are presented and analyzed in Sections 4.2 and 4.3.

4.1 TEST CONDITIONS

These tests were carried out in the showerhead region and the first row of holes on the suction side of the simulated vane. Tests included adiabatic effectiveness tests as well as thermal field measurements. The adiabatic effectiveness tests were all run at a density ratio of $DR = 1.2$ with the coolant temperature at $T_c = 250$ K. Although a density ratio of $DR = 2.0$ are more representative of the actual engine conditions, these tests were run at $DR = 1.2$ as the main aim of the experiments was to find the effects of the hot streak on the coolant effectiveness. Also Ethridge (2000) and Cutbirth (2000) showed that the

lower density ratios are close representations of the effects observed at the higher density ratios.

A variety of blowing ratios ranging from $M^* = 0.8$ to $M^* = 2.0$ were studied in the showerhead region. For the suction side region, blowing ratios ranging from $M = 0.5$ to $M = 1.4$ were studied. These ranges of blowing ratios were chosen as they extend over a range where the adiabatic effectiveness is significant. All the adiabatic effectiveness tests were conducted under the moderate turbulence condition where $Tu = 3.5\%$. For the suction side adiabatic effectiveness tests, the showerhead holes were covered up using thin duct tape. This was used to prevent boundary layer disturbances on the suction side as well as to prevent ingestion of the hot streak as it impacted on the vane.

In a real engine operating environment, coolant from all regions, the showerhead, the suction side and the pressure side, are used to cool the vane. In this thesis, effects of the hot streak occurring in these regions are looked at separately as a first step in understand the effects of the hot streak. In the following chapters, it will be pointed out that the showerhead region is more synonymous with a constant high temperature region near the vane surface and the suction side region corresponds to having a temperature gradient near the vane surface. These separate conditions have to be understood before introducing the additional effects on the hot streak and the film cooling performance downstream

caused by having both the showerhead and the suction side blowing simultaneously.

As the experiments were conducted to find the effect of the hot streak on the coolant effectiveness, the choice of the relevant temperature for the surroundings that is used to calculate the adiabatic effectiveness becomes an important question. This problem is more magnified if there is a temperature gradient that is present off the wall. Measurements of the hot streak temperature and the coolant temperature close to the wall are required to find the relevant surrounding temperature. So, measurements of the thermal field near the wall were performed for both high ($Tu = 20\%$) and moderate ($Tu = 3.5\%$) turbulence conditions, with and without the presence of a hot streak. These results are also discussed in the following sections.

4.2 SHOWERHEAD REGION

The showerhead region is one of the most highly cooled regions in a vane. This is because the heat transfer is really high in this region and also it bears the brunt of the hot streak impact. For the experiments that were carried out in this region, the hot streak was positioned so that it was centered on the stagnation line of the turbine vane.

Measurements of the temperature field near the wall were made at the 1st, 2nd and the 3rd rows of holes on the pressure side of the showerhead, corresponding to positions of $x/d = 0$, $x/d = -3.7$ and $x/d = -7.4$, respectively, where d is the hole diameter. These measurements were done at spanwise locations of $0.49S$ and $0.53S$ where S is the span length of the vane. These locations correspond to the hole centers of holes 7 and 8 as measured from the top of the vane. All measurements were made only at this region as the showerhead region was considered to be unaffected by the buildup of coolant only after this spanwise distance from previous experiments performed by Cutbirth (2000). Temperature measurements were made out to a distance of $5d$ from the wall. As shown by previous measurements by Cutbirth (2000), the coolant jets did not extend beyond $5d$ from the wall in this region.

4.2.1 Moderate Mainstream Turbulence

The temperature profiles measured under moderate turbulence conditions are presented in Figures 4.1 and 4.2. From these figures, it is clear that temperature near the wall is nominally a constant value of $T/T_\infty = 1.10$ for a distance of $5d$. The region under study was under the core of the hot streak.

Adiabatic effectiveness tests were then conducted without the presence of the hot streak. The hot streak was then turned on and the experiments were

repeated with all other conditions remaining the same. These experiments conducted at moderate turbulence, along with the temperature field measurements were used to determine if it was possible to scale the adiabatic effectiveness with a properly adjusted mainstream temperature.

For the laterally averaged adiabatic effectiveness results presented in Figure 4.3, the adiabatic effectiveness levels were determined using a “standard” and an “adjusted” mainstream temperature value. The “standard” adiabatic effectiveness was calculated using the mainstream temperature, while the “adjusted” adiabatic effectiveness was calculated using an apparent mainstream temperature that was equal to the hot streak temperature of $T/T_{\infty} = 1.10$.

From Figure 4.3, it was apparent that the calculation of the coolant effectiveness using the “standard” method did not scale the adiabatic effectiveness levels properly. But the use of an “adjusted” mainstream temperature scaled the adiabatic effectiveness values, which matched the results obtained without the presence of a hot streak. Although the values of the “adjusted” adiabatic effectiveness levels were consistently lower, these differences were within the uncertainty of the experiment of $\delta\eta = \pm 0.05$. The results for blowing ratios of $M^* = 1.0$ and $M^* = 1.6$ plotted in Figure 4.4 show similar agreement in the adiabatic effectiveness levels.

As the adiabatic effectiveness plots shown in Figures 4.3 and 4.4 were averaged adiabatic effectiveness values, a good correspondence of these plots alone did not ensure a proper scaling temperature. The local adiabatic effectiveness values also had to match up for both these cases. Therefore, local adiabatic effectiveness contours were plotted for all these blowing ratios and their values were compared.

Figure 4.5 shows the adiabatic effectiveness contour for a blowing ratio of $M^* = 2.0$. From the figure, it was clear that the adiabatic effectiveness contours for the “adjusted” mainstream temperature case were very similar to the contour levels obtained without the use of a hot streak. But this similarity was no longer apparent further downstream, beyond $x/d = 15$. Based on earlier measurements presented in Chapter Three, the hot streak decays as it passes around the vane. As the temperature field was not measured this far downstream, the decay in the hot streak temperature was not accounted for and this resulted in the drop in the “adjusted” levels.

4.2.2 High Mainstream Turbulence

Measurements of the thermal field were also carried out under high mainstream turbulence conditions to assess the effects of mainstream turbulence. These measurements are plotted in Figures 4.7 and 4.8. In the region of coolant

separation, which was a distance of $5d$ from the wall, the temperature ratio was still a constant value. Based on the results obtained for the moderate turbulence case, it was evident that a similar use of the constant hot streak temperature would scale the adiabatic effectiveness values and so adiabatic effectiveness measurements were not conducted at high turbulence.

4.3 SUCTION SIDE REGION

To find the effect of a temperature gradient of the wall, measurements were made of the effects on the hot streak on the adiabatic effectiveness of the first row of holes on the suction side of the vane. This row of holes was positioned at $25d$ downstream of the stagnation line. This hole location was designated as $x'/d = 0$. The measurement of the hot streak presented in Chapter Three indicated that the hot streak was compressed at this location, suggesting the possibility of sharp gradients being present of the wall. The hot streak was again centered on the stagnation line as this provided the maximum gradient off the wall.

4.3.1 Moderate Mainstream Turbulence

The temperature profiles that were obtained at moderate turbulence on the suction side region are shown in Figures 4.9 and 4.10. Figure 4.9 shows

approximately a 25% decrease in hot streak temperature at a distance of $2d$ and a 50% decrease at a distance of $5d$ from the surface relative to the surface temperature. Figure 4.10 shows a similar temperature gradient near the wall for varying spanwise positions. The drop in temperatures in the spanwise direction was a result of the temperature profile of the hot streak at this location as described in Chapter Three. As a result there was no “equivalent” mainstream temperature that was immediately apparent as it was in the case for the showerhead region.

As an initial approach to obtain the proper “adjusted” temperature, it was hypothesized that the temperature at the outer boundary of the coolant jet could be the right temperature. To determine this temperature, measurements were made of the temperature profile in the near wall region with the coolant jets blowing at various blowing ratios. These measurements, made at a spanwise location of $z = 0.47S$, were at a position coincident with the centerline of a coolant jet and are shown in Figure 4.11. Also, to determine the effect of the hot streak on this coolant, temperature measurements were made with the hot streak turned on and these are represented in Figure 4.12. Although these measurements were not able to precisely indicate the distance of separation, they did indicate that the outer edge of the coolant did not extend more than a distance of $y/d = 0.5$ for $M^* = 0.6$, and $y/d = 1.2$ for $M^* = 1.0$ and 1.2 .

The temperature ratio of the coolant on interaction with the hot streak was $T/T_\infty = 1.085$ at a distance of $y/d = 1.2$ as compared to the temperature ratio of $T/T_\infty = 1.095$ at the surface with the hot streak and no film cooling. The differences in the adiabatic effectiveness levels calculated based on these different temperature ratios were within the experimental uncertainty. So it was decided that the surface temperature measured with the hot streak and no film cooling would be used as the adjusted equivalent mainstream temperature for the adiabatic effectiveness.

Different approaches were followed to obtain the equivalent mainstream temperature. Based on the required adiabatic effectiveness, the local mainstream temperatures that would scale the adiabatic effectiveness values to match those obtained for the case without the hot streak were back calculated. These temperatures were then compared with the surface temperature measurements. These temperatures were calculated for various blowing ratios to understand the effect of a change in the blowing ratio.

Tables 4.1 and 4.2 show the required mainstream temperature and the difference between the required temperature and the temperature obtained using the surface thermocouple. The average temperature is an average of the required temperatures as calculated for the different blowing ratios. Temperature

differences between the required temperature for different blowing ratios and the surface temperatures are also tabulated.

Table 4.1 : Surface temperature comparison at $x'/d = 7$

z/d	Measured Temperature (Tm)	Average Required Temperature (Tr)	$\Delta T (Tr - Tm)$		
			M = 0.6	M = 0.8	M = 1.2
11.1	328.93	330.67	11.07	-0.93	-4.93
5.55	326.73	325.33	-5.73	-1.73	3.27
0	322.35	325.00	7.65	-1.35	1.65

Table 4.2 : Surface temperature comparison at $x'/d = 14$

z/d	Measured Temperature (Tm)	Average Required Temperature (Tr)	$\Delta T (Tr - Tm)$		
			M = 0.6	M = 0.8	M = 1.2
11.1	323.27	326.00	5.73	3.73	-1.27
5.55	322.09	322.67	1.91	0.91	-1.09
0	318.93	313.33	-2.93	-6.93	-6.93

From the two tables, it was evident that there was no particular trend in the required temperatures. This table also indicated that the required temperature needed to be lower in certain cases and higher in certain cases in a random fashion. From these results, it was concluded that any one of the surface temperature measurements alone could not be used to scale the adiabatic effectiveness measurements for this region.

To obtain the proper “adjusted” temperature required the surface temperatures of the vane. But these measurements were performed only at nine discrete point locations. To obtain the surface temperatures at intermediate

locations, the available data was interpolated. From the surface temperature measurements obtained using the thermocouple rake, a curve fit was obtained to provide the surface temperatures for various streamwise and spanwise locations. Curve fits were generated for the spanwise and the streamwise decay separately. The temperatures that were obtained using this curve as compared to the actual surface temperatures measured by the thermocouple rake are shown in Figure 4.13. As a single curve fit was used to account for both the spanwise and the streamwise decay, the curve fit temperatures did not match up to the same extent with the surface thermocouple measurements in all the different regions.

Figure 4.14 shows a plot of the averaged adiabatic effectiveness levels for a blowing ratio of $M = 0.5$, calculated using an “adjusted” mainstream temperature and the “standard” mainstream temperature along with the adiabatic effectiveness levels observed in the absence of a hot streak. For this case, the standard adiabatic effectiveness levels were calculated using the mainstream temperature and the adjusted adiabatic effectiveness levels were calculated using an apparent mainstream temperature obtained using the procedure described above. From the figure, it was clear that the “adjusted” adiabatic effectiveness levels were a closer representation of the adiabatic effectiveness levels obtained without any hot streak. A similar procedure to calculate the “adjusted” adiabatic effectiveness levels was followed for different blowing ratios and Figure 4.15

shows a plot of these adiabatic effectiveness levels for blowing ratios of $M = 0.6$ and $M = 1.2$. The adiabatic effectiveness values differed by a maximum value of $\delta\eta = 0.07$ in the regions close to the hole corresponding to $x/d < 3$ and in the region far downstream corresponding to $x/d > 13$ and were within the uncertainty of $\delta\eta = 0.03$ in other regions.

As in the case of the showerhead region, the local adiabatic effectiveness contours were also checked. Figures 4.16 and 4.17 show the local adiabatic effectiveness distributions for $M = 0.6$. For the hot streak case, an “adjusted” mainstream temperature was used to calculate the adiabatic effectiveness. These contours indicated that the local adiabatic effectiveness values were reasonably similar for both the hot streak and the no hot streak case when using appropriately adjusted mainstream temperatures.

The hot streak temperatures were measured with the use of a thermocouple rake based on the assumption that the off wall measurements would provide us with the right “adjusted” mainstream temperature. So, the surface measurements were performed only at point locations, and thus the measurement technique had limitations in resolving the surface temperatures. These were also compounded by the measurement errors that were introduced during the adiabatic effectiveness calculation procedure with and without the hot streak as discussed in Chapter Two. These limitations in the measurement techniques prohibited the

precise calculation of an “adjusted” mainstream temperature that would scale the adiabatic effectiveness levels. But the present method of calculating the “adjusted” mainstream temperature was still able to scale the averaged adiabatic effectiveness and was also able to resolve the local adiabatic effectiveness values reasonably well.

4.3.2 High Mainstream Turbulence

Experiments were also conducted with high mainstream turbulence in which the temperature profile within the hot streak near the wall was measured in the region downstream of the first suction side coolant holes. From Figure 4.17, it was clear that the change in the temperature ratio of the coolant even for a distance of $y/d = 2$ from the wall were less than 10%. Since the temperature gradients near the wall for the high mainstream turbulence case were less than that for the moderate mainstream turbulence case. Consequently, the surface temperature would provide the “adjusted” mainstream temperature required to scale the adiabatic effectiveness values and so no additional adiabatic effectiveness tests were done for high mainstream turbulence.

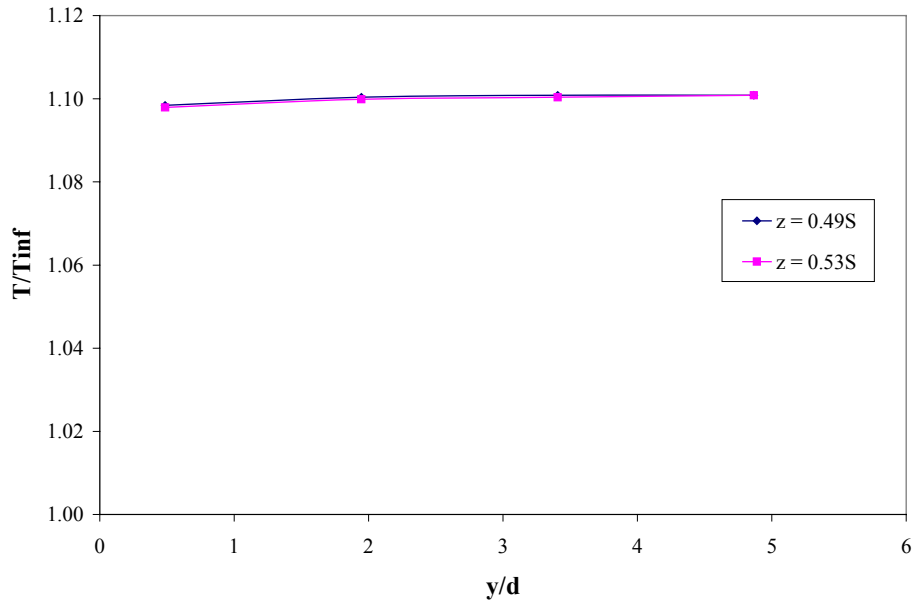


Figure 4.1 : Temperature ratio measured in the showerhead region under moderate turbulence showing the spanwise variations.

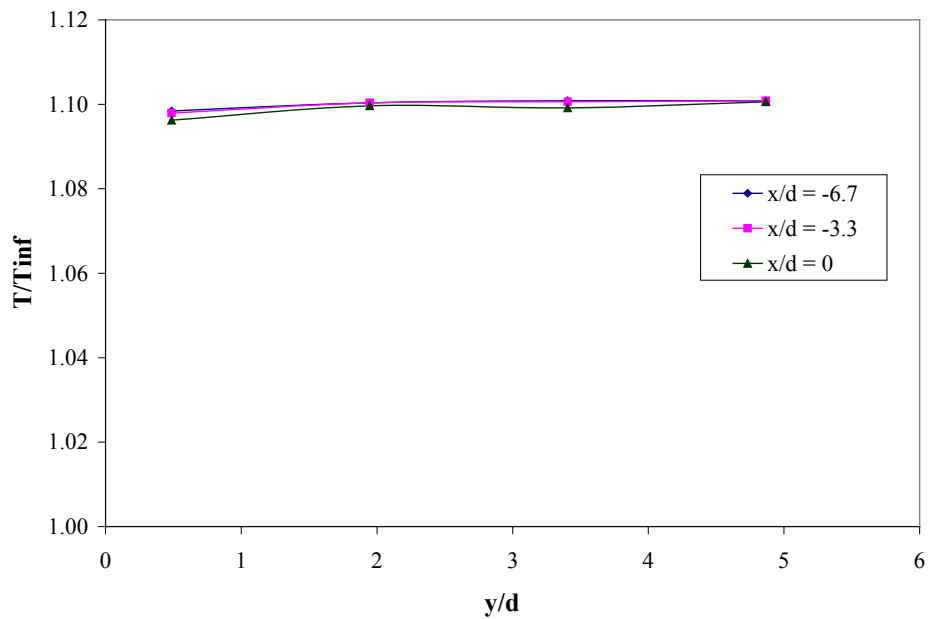


Figure 4.2 : Temperature ratio measured in the showerhead region under moderate turbulence showing the streamwise variations.

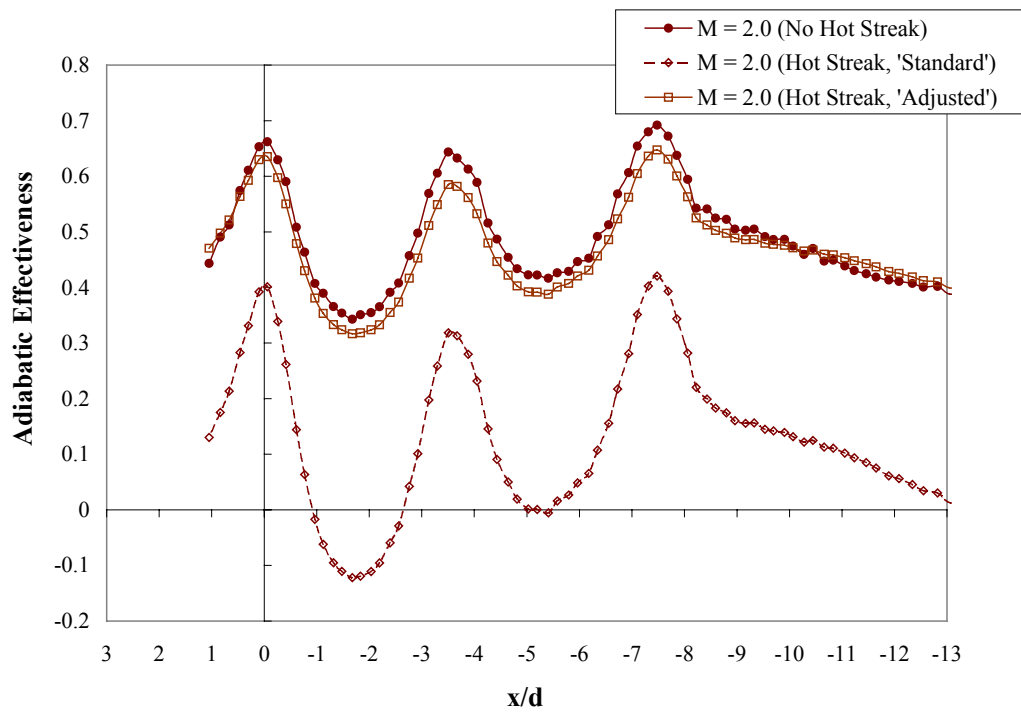


Figure 4.3 : Adiabatic effectiveness in the showerhead region at a DR = 1.2, M = 2.0 under moderate turbulence conditions with and without the hot streak

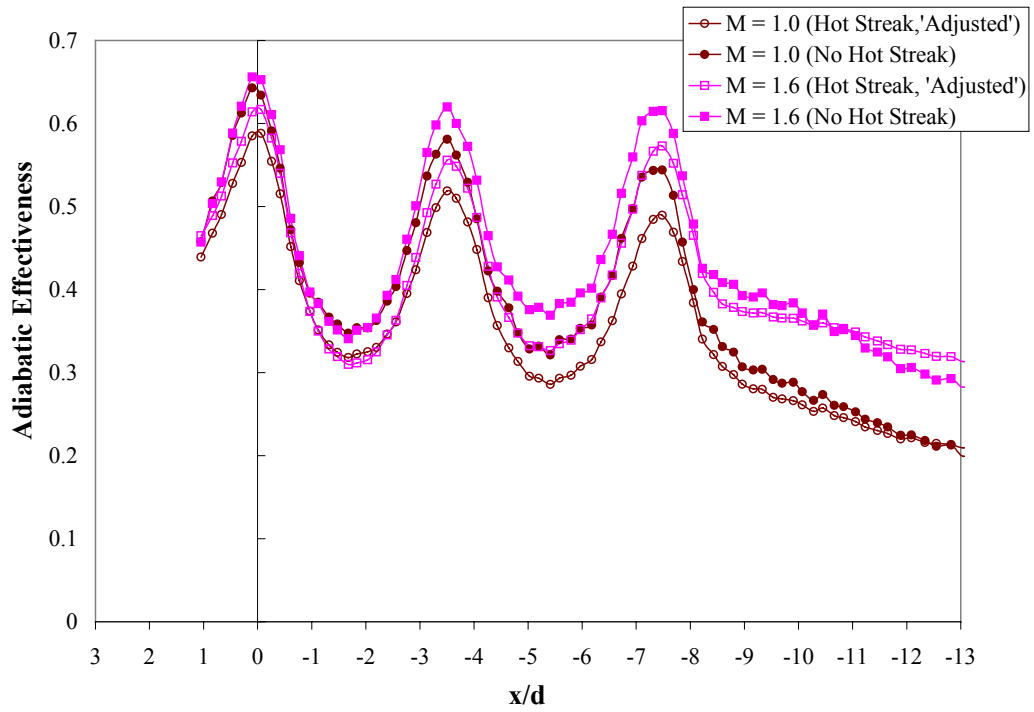


Figure 4.4 : Adiabatic effectiveness in the showerhead region at a DR = 1.2, and $M = 1.0$ and $M = 1.6$ under moderate turbulence conditions with and without the hot streak

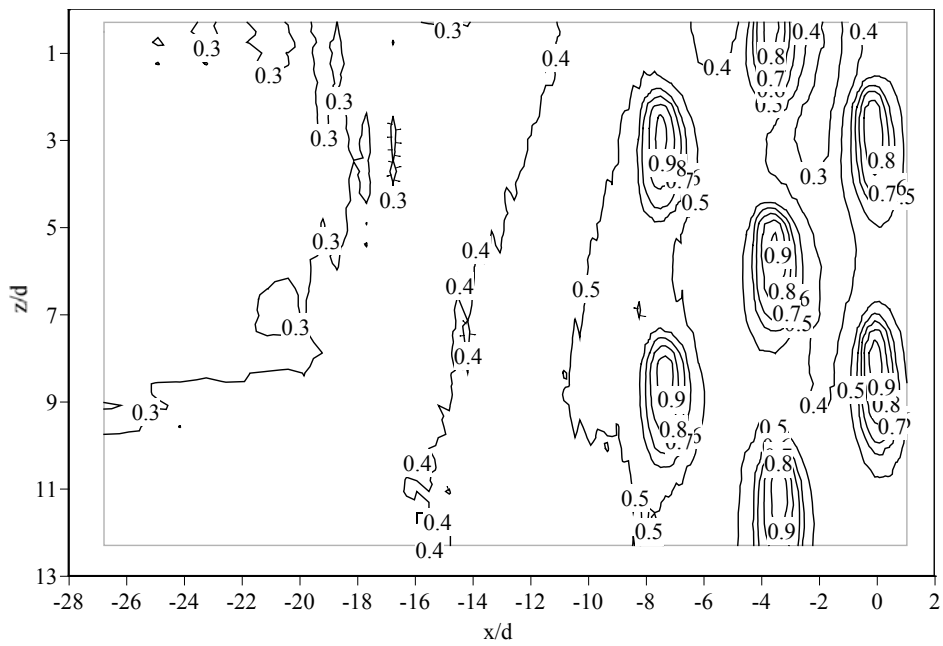


Figure 4.5 : Contour levels of local effectiveness values in the showerhead under moderate turbulence condition without a hot streak.

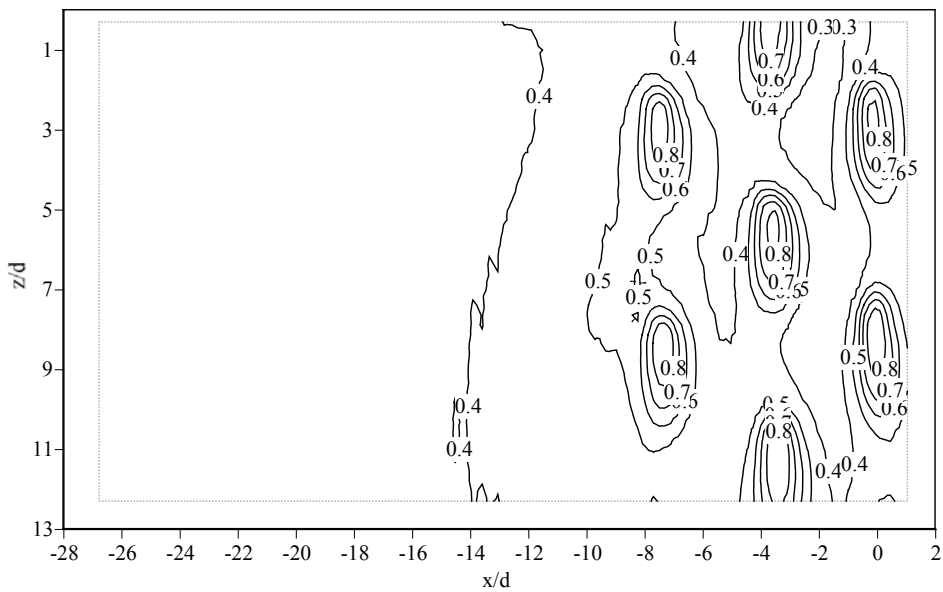


Figure 4.6 : Contour levels of local effectiveness values in the showerhead under moderate turbulence condition with a hot streak.

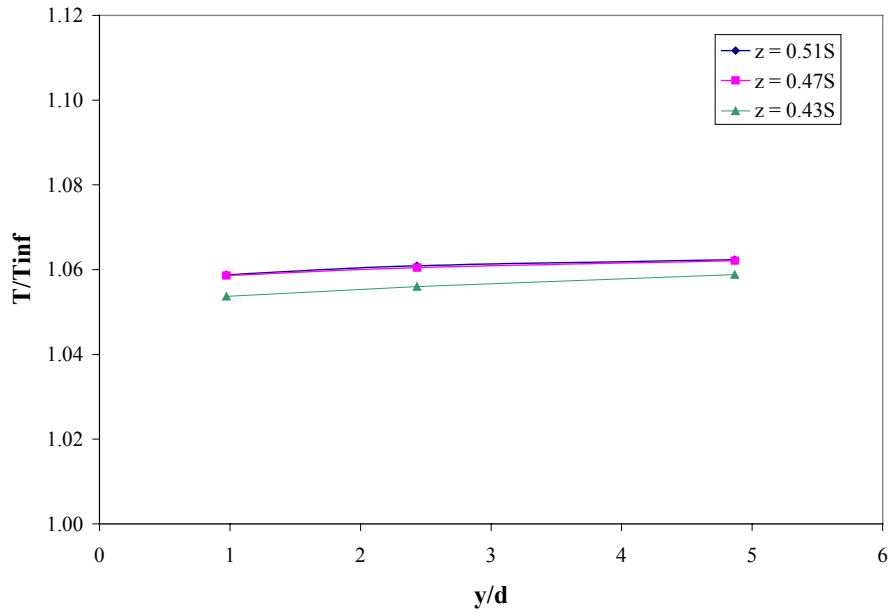


Figure 4.7 : Temperature ratio measured in the showerhead region at $x/d = 0$ under high turbulence conditions showing the spanwise variations.

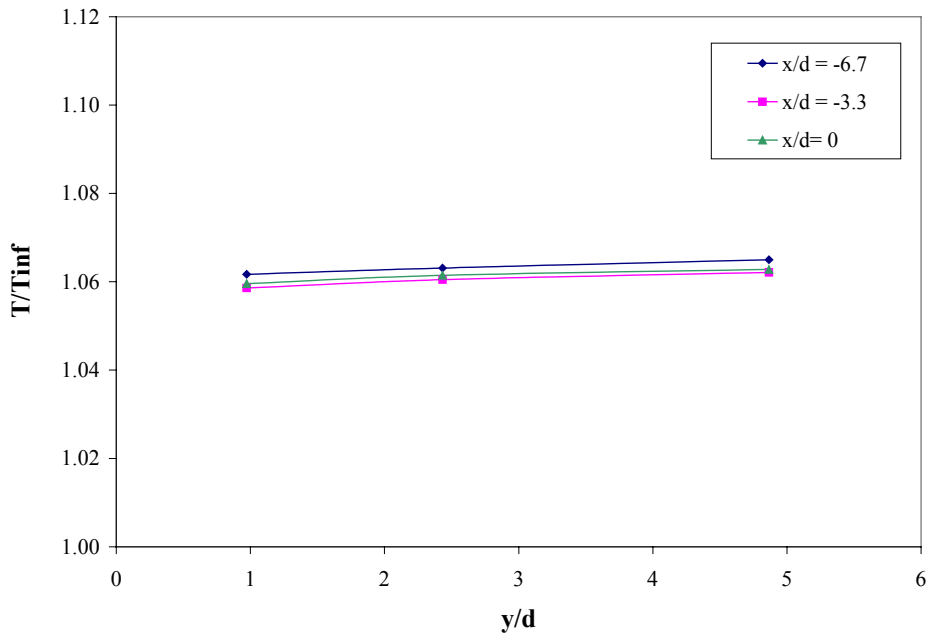


Figure 4.8 : Temperature ratio measured in the showerhead region at $z = 0.47S$ under high turbulence conditions showing the streamwise variations.

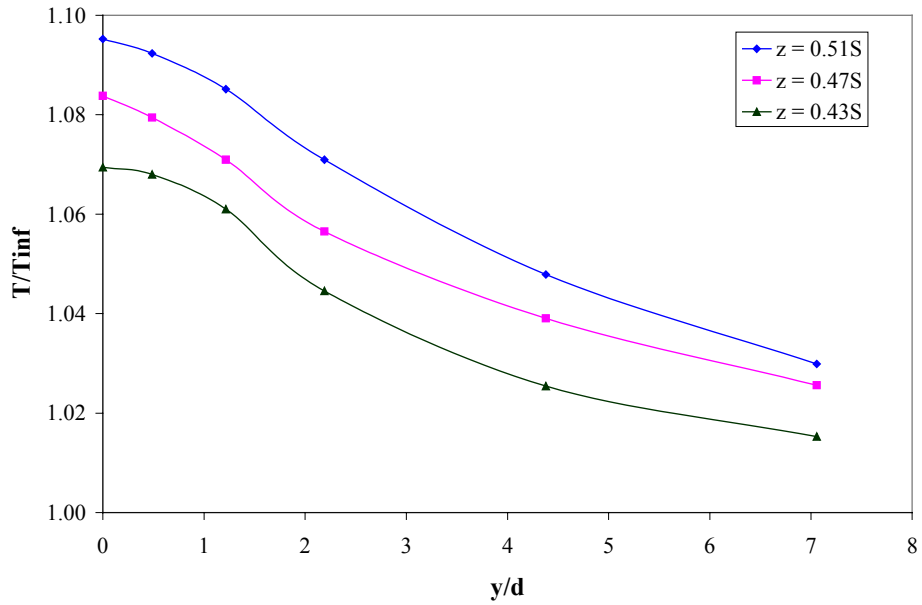


Figure 4.9: Temperature ratio measured on the suction side at $x'/d = 0$ with just the hot streak under moderate turbulence.

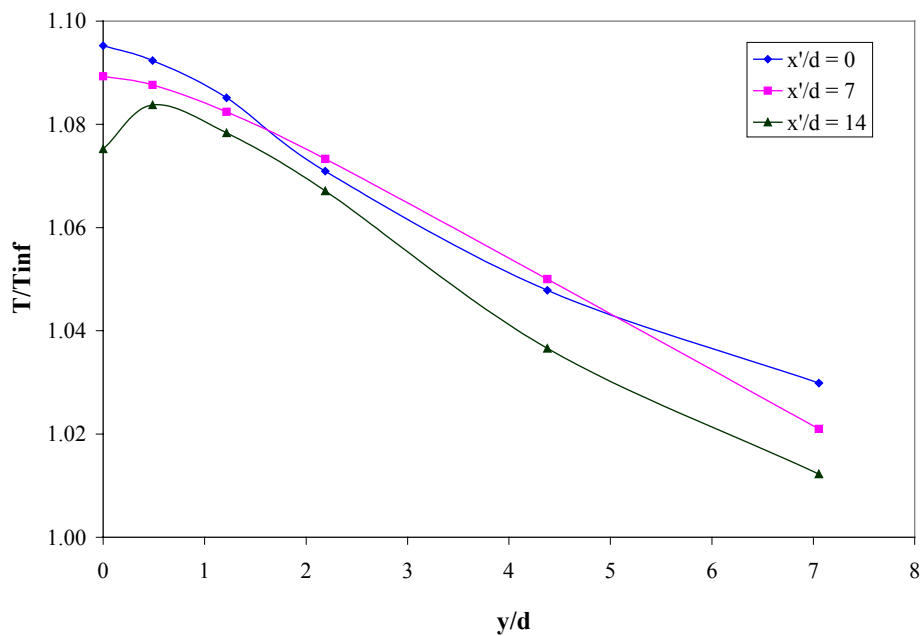


Figure 4.10 : Temperature ratio measured on the suction side at $z = 0.51S$ with just the hot streak under moderate turbulence.

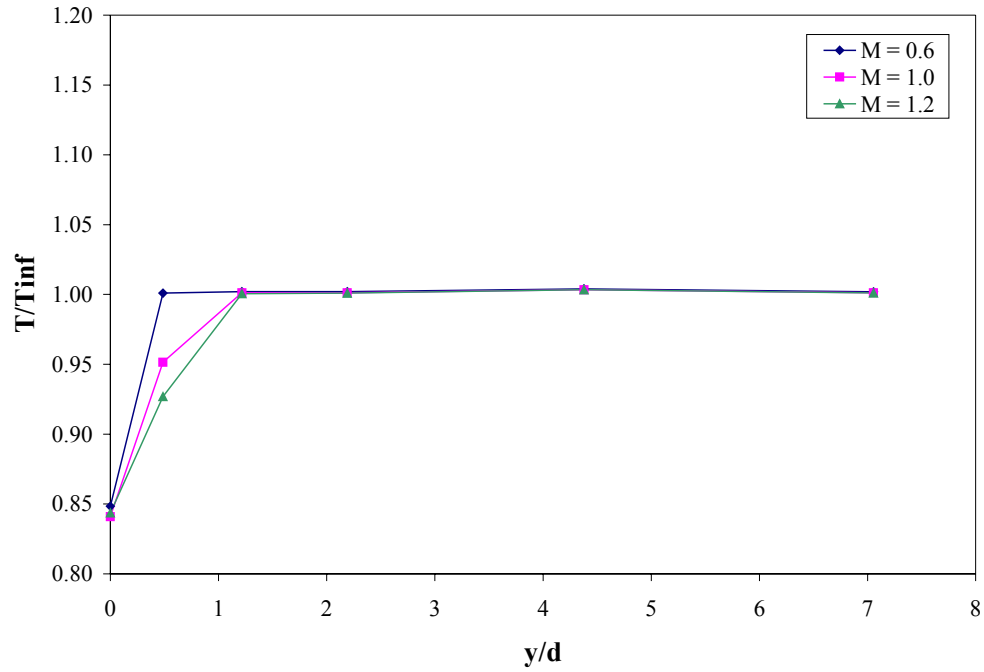


Figure 4.11 : Temperature ratio measured on the suction side at $z = 0.51S$ and at $x'/d = 0$, with coolant at a density ratio of 1.2, without the presence of a hot streak.

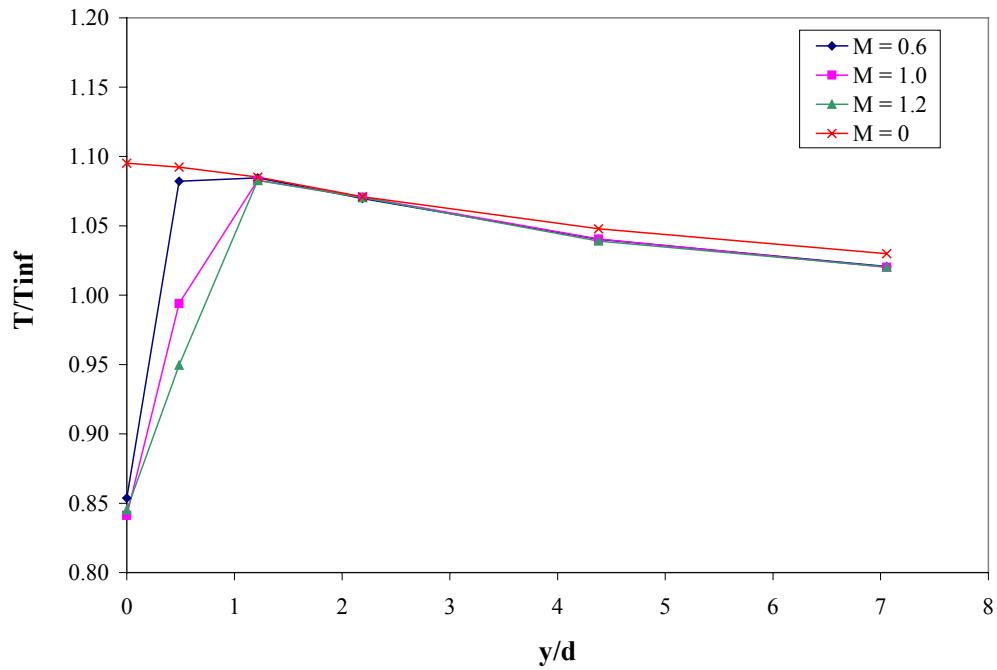


Figure 4.12 : Temperature ratio measured on the suction side at $z = 0.51S$ and at $x'/d = 0$, with coolant at a density ratio of 1.2 in the presence of a hot streak.

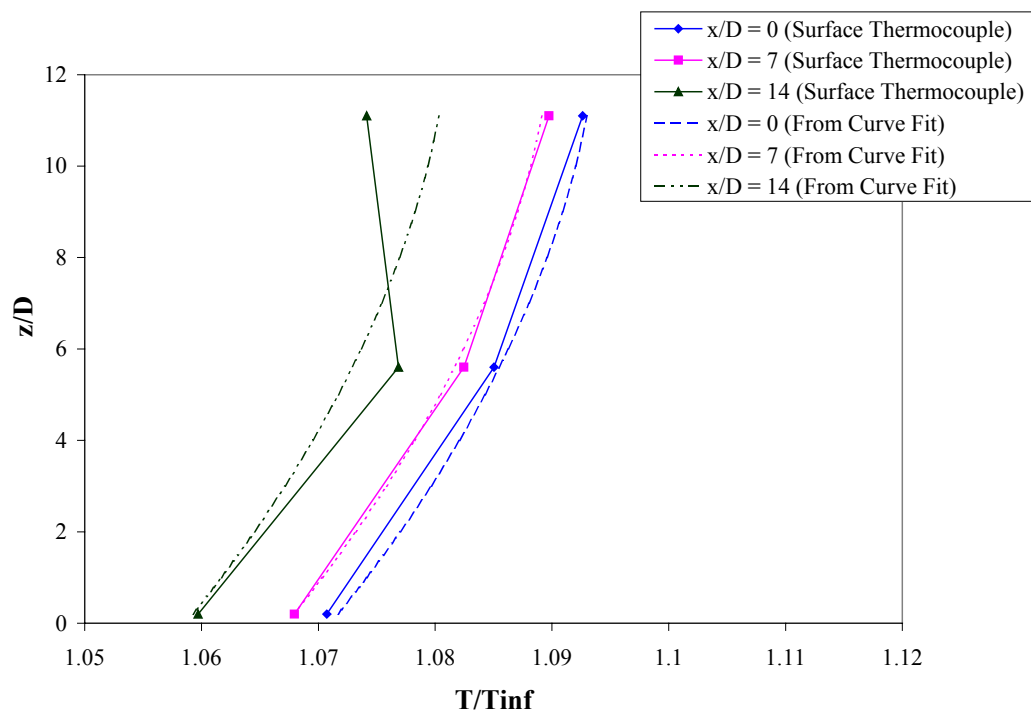


Figure 4.13 : Comparison of vane surface temperatures under the influence of a hot streak as measured by a thermocouple rake and as calculated using a curve fit of temperatures.

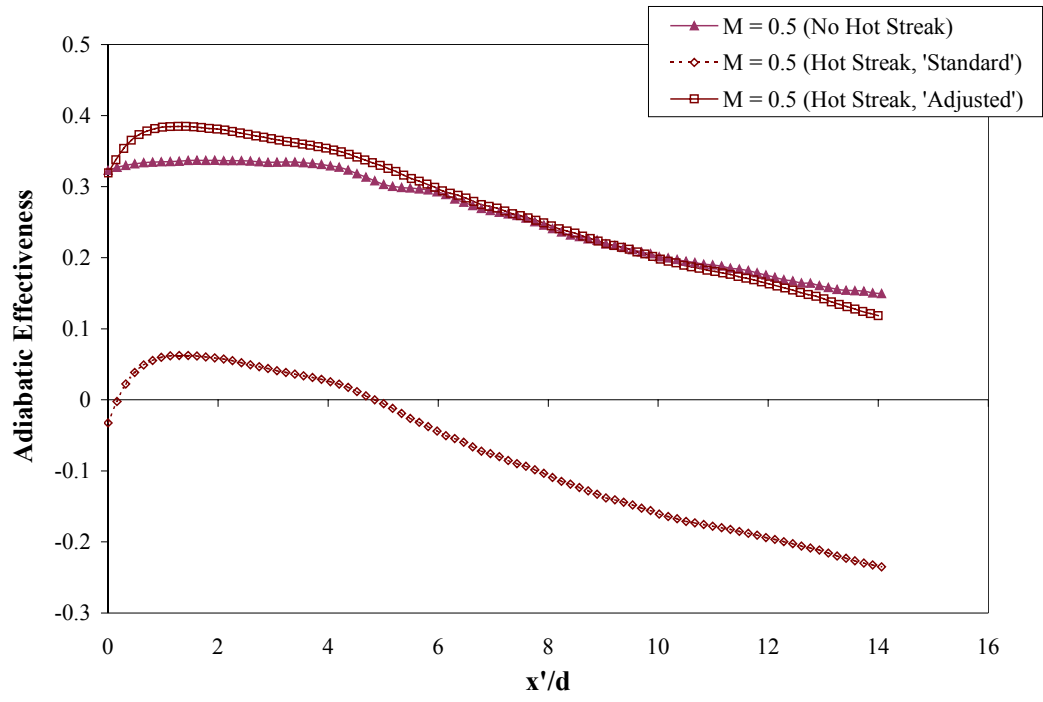


Figure 4.14 : Adiabatic Effectiveness in the suction side for 1 row of holes blowing at a density ratio of 1.2 and blowing ratio of 0.5 under moderate turbulence.

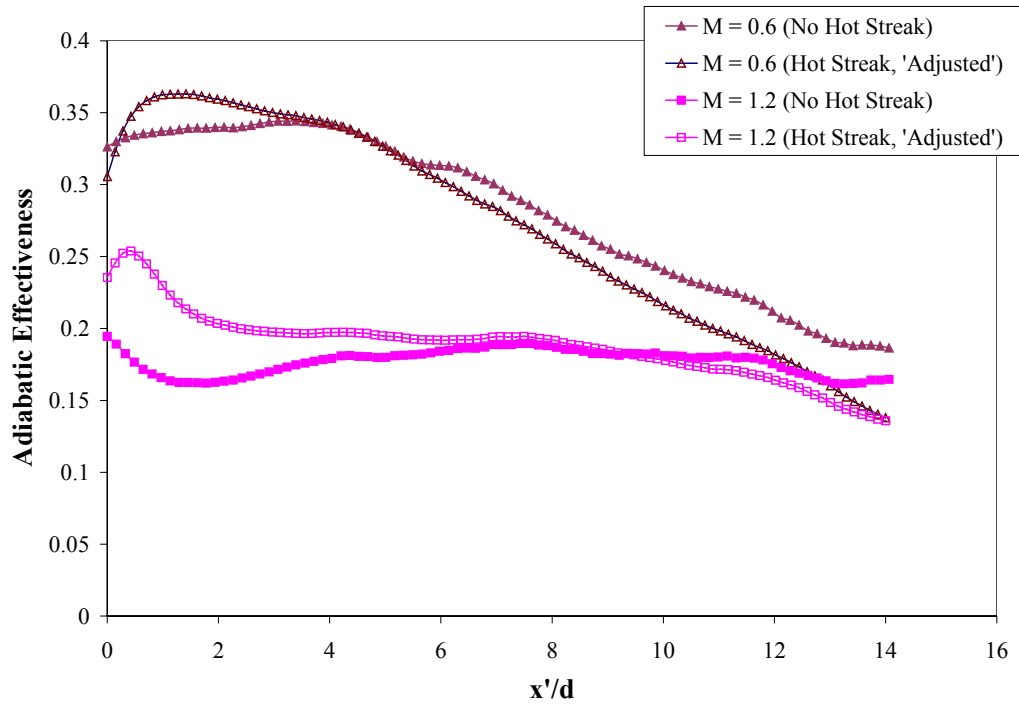


Figure 4.15 : Adiabatic Effectiveness in the suction side for 1 row of holes blowing at a density ratio of 1.2 under moderate turbulence for blowing ratios of 0.6 and 1.2.

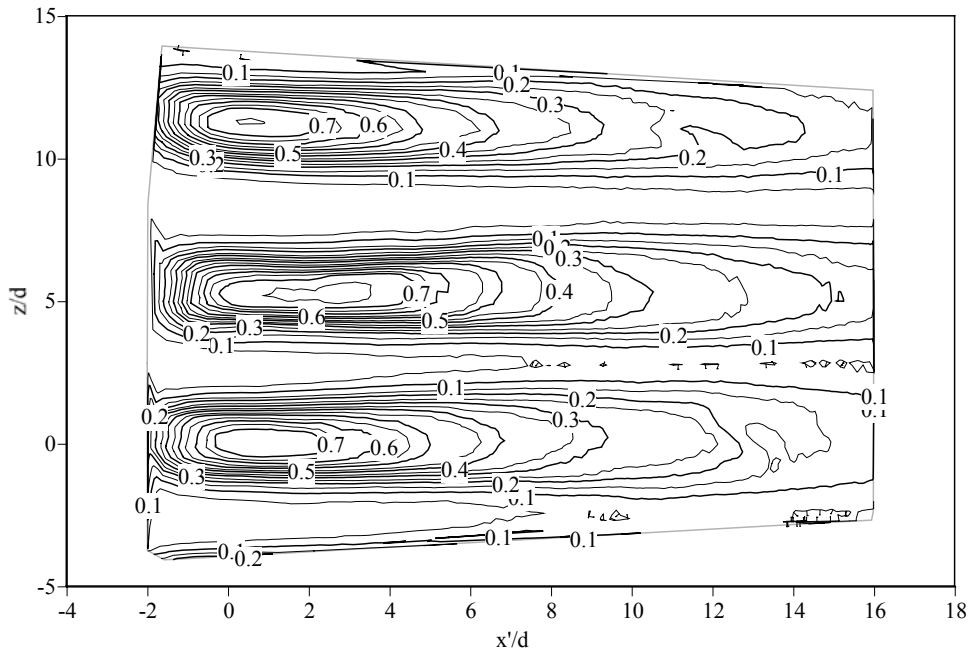


Figure 4.16 : Contour levels of local effectiveness values in the suction side under moderate turbulence condition without the presence of a hot streak.

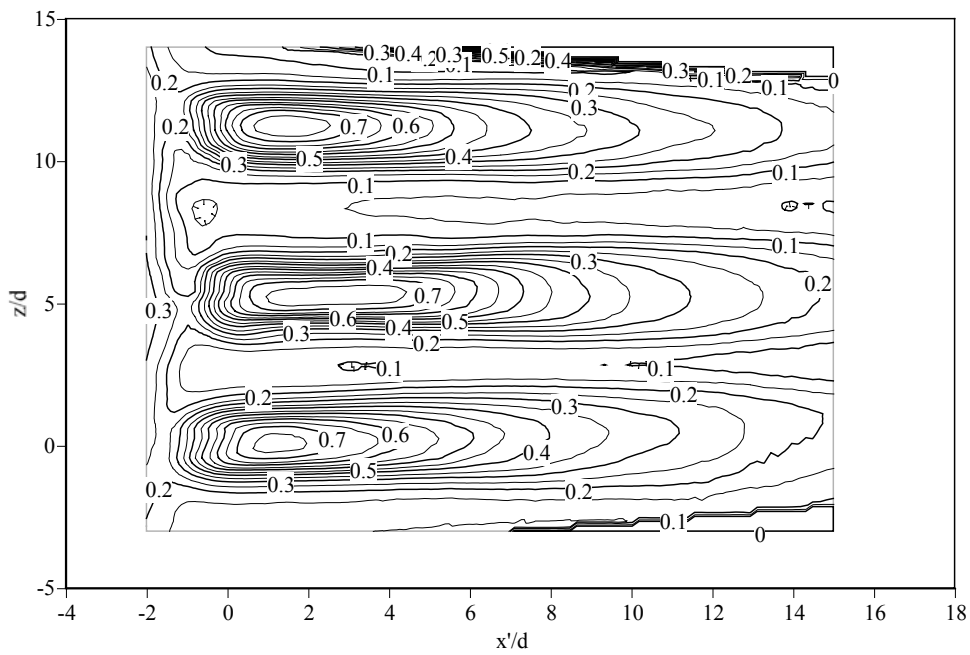


Figure 4.17 : Contour levels of local effectiveness values in the suction side under moderate turbulence condition with a hot streak using an “adjusted” temperature.

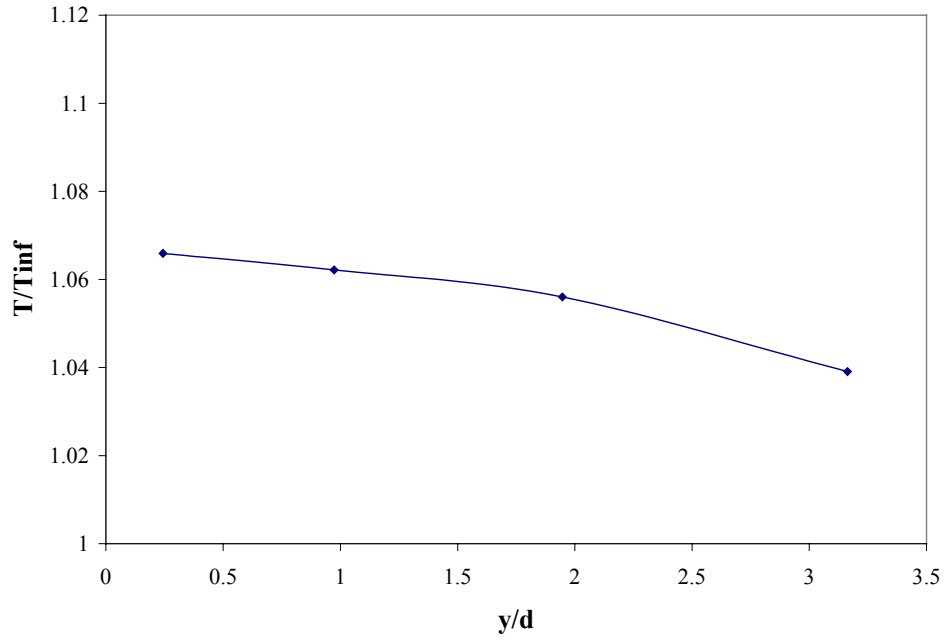


Figure 4.18 : Temperature ratio measured on the suction side at 0.51S with just the hot streak under high turbulence.

CHAPTER FIVE

CONCLUSIONS

5.1 SUMMARY OF RESULTS

From the experiments conducted with the hot streak, it was concluded that mainstream turbulence had a major effect on the strength of the hot streak. The effects of turbulence alone had reduced the peak temperature ratio of the hot streak to half its value measured upstream of the vane. The difference between high turbulence ($Tu = 20\%$) and moderate turbulence ($Tu = 3.5\%$) in the peak normalized temperature ratio measured at the reference wake location was only 20%, although as expected the high turbulence profile showed more spreading of the hot streak.

It was also confirmed that the positioning or clocking of the hot streak did not change the hot streak temperature profile measured in the wake although the temperature profile measured for the impacting hot streak was more coherent. This indicated the suppression of turbulence near the vane walls that helped make the hot streak more coherent.

Measurements of the hot streak temperatures in the showerhead region showed a uniform hot streak temperature until a distance of $5d$ from the wall. The

use of an “adjusted” mainstream temperature to scale the effectiveness proved to be successful for this uniform temperature field. Both averaged effectiveness and local effectiveness contours compared well for the cases with and without the hot streak.

Measurements of the hot streak temperatures near the vane surface on the suction side indicated a sharp gradient in the temperatures. It was decided, based upon the analysis of the measured temperature levels, that the surface temperature obtained with a hot streak in the absence of film cooling would be used to calculate the “adjusted” mainstream temperature. Curve fits were used based on the point temperature measurements obtained on the surface using a rake, to find the local surface temperature. The adiabatic effectiveness levels and the effectiveness contours that were obtained by this method were reasonably similar to the values obtained without the presence of a hot streak.

From these experiments, it was concluded that the adiabatic effectiveness of the coolant in the presence of a hot streak can be scaled to match the adiabatic effectiveness levels obtained without a hot streak if the right mainstream temperature was used. The value of this temperature, though, depended on the measurement region of the vane and the temperature profile of the hot streak in that region.

5.2 RECOMMENDED FUTURE WORK

One of the limiting factors in calculating an adjusted temperature on the suction side was the thermal resolution of the surface temperatures that was required. As it has been established that the vane surface temperatures are probably more relevant in calculating the adjusted mainstream temperature, a more detailed surface temperature field with the hot streak can be measured by using infra red images and these can then be used to identify the relevant mainstream temperature.

In the actual engine, film cooling from all the three regions, the showerhead, the suction side and the pressure side are used to cool the vane. So the effects of the hot streak on the suction side coolant effectiveness, with the showerhead blowing at the same time can also be investigated.

References

Butler, T. L., Sharma, O. P., Joslyn, H. D., and Dring, R. P., 1989, "Redistribution of an Inlet Temperature Distortion in an Axial Flow Turbine Stage," *Journal of Propulsion and Power*, Vol. 5, No. 1, pp. 64-71.

Cutbirth, J.M., 2000, "Turbulence and Three-Dimensional Effects on a Film Cooled Turbine Vane," Ph.D. Dissertation, The University of Texas at Austin.

Ethridge, M.I., 2000, "Suction Side Film Cooling of a First Stage Gas Turbine Vane," M.S. Thesis, The University of Texas at Austin.

Dorney, D. J., Davis, R. L., Sharma, O.P., 1991, "Two-Dimensional Inlet Temperature Profile Attenuation in a Turbine Stage" ASME Paper 91-GT-406

Dorney, D. J., 1997, "Investigation of Hot Streak Temperature Ratio Scaling Effects," *International Journal of Turbo and Jet Engines*, Vol. 14, pp. 217-227.

Dorney, D. J., Gundy-Burlet, K. L., Sondak, D. L., 1999, "Survey of Hot Streak

Experiments and Simulations,” International Journal of Turbo and Jet Engines, Vol. 16, No. 1, pp. 1-15.

Dorney, D.J., Davis, R.L., Edwards, D.E., and Madavan, N.K., “Unsteady Analysis of hot streak migration in a Turbine Stage,” Journal of Propulsion and Power, Vol. , No.2, pp. 520-529.

Dorney, D.J., and Gundy Bulet, K.L., 1996, “Hot Streak Clocking Effects in a 1-1/2 Stage Turbine,” Journal of Propulsion and Power, Vol 12, No.3, pp 619-620.

Dorney, D.J., and Davis, R.L., 1993, “Numerical Simulation of Turbine ‘Hot Spot’ Alleviation Using Film Cooling,” Journal of Propulsion and Power, Vol. 9, No. 3, pp. 329-336.

Je-Chin Han, Sandip Dutta, and Srinath V. Ekkad, “Gas Turbine Heat Transfer and cooling technology”.

Jenkins, S., Krishnakumar, V., Bogard, D.G., 2003, “The Effects of Mainstream Turbulence And Turbine Vane Film Cooling on the Dispersion of a Hot

Streak,” Proceedings of the 2003 ASME Turbo Expo, Paper No. GT2003-38575

Polanka, M.D., 1999, “Detailed Film Cooling Effectiveness and Three Component Velocity Field Measurements on a First Stage Turbine Vane Subject to High Freestream Turbulence,” Ph.D. Dissertation, The University of Texas at Austin.

Roback, R.J. and Dring R.P., 1993, “Hot Streaks and Phantom Cooling in a Turbine Rotor Passage: Part I – Separate Effects,” Journal of Turbomachinery, Transactions of the ASME, Vol.115, No. 4, pp. 651-666.

Roback, R.J. and Dring R.P., 1993, “Hot Streaks and Phantom Cooling in a Turbine Rotor Passage: Part II – Combined Effects and Modeling,” Journal of Turbomachinery, Transactions of the ASME, Vol.115, No. 4, pp. 667-681.

Schwab, J. R., Stabe, R. G., and Whitney, W. J., 1983, “Analytical and Experimental Study of Flow Through an Axial Turbine Stage with Nonuniform Inlet Radial Temperature Profiles,” NASA Technical Memorandum 83431, AIAA 83-1175.

Shang, T. and Epstein, A.H., 1997, "Analysis of hot streak effects on turbine rotor heat load," *Journal of Turbomachinery, Transactions of the ASME*, Vol. 119, No.3, pp. 544-553.

Stabe, R. G., Whitney, W. J., and Moffitt, T. P., 1984, "Performance of a High-Work Low Aspect Ratio Turbine Tested with a Realistic Inlet Radial Temperature Profile," *NASA Technical Memorandum 83655, AIAA Paper No. 84-1161*.

Takahashi, R. and Ni, R.H., 1990, "Unsteady Euler Analysis of the Redistribution of an Inlet Temperature Distortion in a Turbine," *AIAA Paper 90-2662*.

VITA

Krishnakumar Varadarajan was born in Chennai, India on March 8, 1980 to Varadarajan Raghavachari and Janaki Varadarajan. He completed his high school education at Padma Seshadri Bala Bhavan Senior Secondary School in his hometown in 1997. He then entered the University of Madras for his Bachelor of Engineering degree in Mechanical Engineering and graduated in May 2001. He then joined the graduate school in August 2001 to pursue his Master of Science degree in Mechanical Engineering at The University of Texas at Austin.

Permanent address : B7, Giri Apts, 26-A, Arcot Road,
Virugambakkam, Chennai 600 092
Tamil Nadu, India

This thesis was typed by the author.